UNIVERSITY OF OKLAHOMA

GRADUATE COLLEGE

ANALOG FREE-SPACE OPTICAL LINKS

A Dissertation

SUBMITTED TO THE GRADUATE FACULTY

in partial fulfillment of the requirements for the

degree of

Doctor of Philosophy

By

Hakki Hejjo Refai
Norman, Oklahoma
2005

ANALOG FREE-SPACE OPTICAL LINKS

A Dissertation APROVED FOR THE
SCHOOL OF ELECTRICAL AND COMPUTER ENGINEERING

BY

_____
Dr. James J. Sluss, Jr.

_____
Dr. Pramode K. Verma

_____
Dr. John E. Fagan

_____
Dr. Monte P. Tull

_____
Dr. William O. Ray

Acknowledgements

I would like to acknowledge several people for helping and supporting me during my doctoral work. I would like to sincerely thank my advisor, Prof. James J. Sluss Jr., for his generous time and dedication. He encouraged me to keep developing my research skills and independent thinking during my doctoral process. He continuously motivated my analytical thinking and significantly assisted me with scientific writing. I have learned much from him; without his help and support, I could not have completed my dissertation successfully.

I am also very grateful to my doctoral committee and wish to thank Pramode K. Verma, John E. Fagan, Monte P. Tull, and William O. Ray for their support and professional advice. Special thanks to Dr. Verma who provides guidance for all Ph.D. students in our department. Also, special thanks to Dean Ray for his generosity and support throughout my work with him as a graduate assistant.

Finally, I would like to thank my parents and my brothers for their continuous encouragements.

June 8, 2005

Table of Contents

List of Illustrations

Hakki Refai's Publications

Journal Papers:

Hakki H. Refai, James J. Sluss, Jr., Hazem H. Refai, and Mohammed Atiquzzaman, "A comparative study of performance of analog fiber-optic links versus free-space optical links," Accepted to SPIE Optical Engineering.

Conference Papers with Proceedings

Hakki. H. Refai, James. J. Sluss, Jr., M. Atiquzzaman, H. Nguyen and D. Ngo, "Analog and digital avionics signal distribution using WDM," Accepted to IEEE 24th Digital Avionics Systems Conference (DASC), Washington, D.C., October 30-November 3, 2005.

Hakki H. Refai, James J. Sluss, Jr., and Hazem H. Refai, "The use of free-space optical links for CATV applications," Proceedings of the SPIE Opto Ireland, Vol. 5825, Dublin, Ireland, April 4-5, 2005.

Hakki H. Refai, James J. Sluss, Jr., and Hazem H. Refai," The transmission of multiple RF signals in free-space optics using wavelength division multiplexing,"

Proceedings of the SPIE Defense and Security Symposium 2005, Vol. 5793, Orlando, FL, March 18–April 1, 2005.

Hakki H. Refai, James J. Sluss, Jr., and Hazem H. Refai, "Free-space optical communication performance in the presence of interfering laser signals," Proceedings of the SPIE Defense and Security Symposium 2005, Vol. 5793, Orlando, FL, March 18–April 1, 2005.

Hakki H. Refai, James J. Sluss, Jr., Hazem H. Refai, and Mohammed Atiquzzaman, "Transporting RF signals over free-space optical links," Proceedings of the SPIE Photonics West 2005, Vol. 5712, San Jose, CA, January 22-27, 2005.

Hakki. H. Refai, James. J. Sluss, Jr., M. Atiquzzaman, H. Nguyen and D. Ngo, "The application of fiber optic wavelength division multiplexing in RF avionics," Proceedings of the IEEE 23rd Digital Avionics Systems Conference (DASC), Salt Lake City, UT, October 24-28, 2004- pp. 8.D.1-1 to 8.D.1-8.

Hakki H. Refai, James. J. Sluss, Jr., Hazem H. Refai, "Interconnection of IS-95 CDMA microcells using free-space optical links," Proceedings of the 1st IEEE and IFIP International Conference on Wireless and Optical Communications Networks (WOCN 2004), Muscat, Oman, June 7-10, 2004, pp. 78-81.

Conference Papers with Abstract/Summary

Hakki. H. Refai, James. J. Sluss, Jr, and Hazem. H. Refai, "Optical interference on free-space optical transceivers," Presented at Frontiers in Optics – 87th Optical Society of America Annual Meeting, Tuscon, AZ, October 5-9, 2003- pp. WJJ6.

Abstract

Free-space optics (FSO) communications is a technology that uses modulated infrared optical beams to transmit information line-of-sight through the atmosphere. There has been a substantial increase in the use of FSO technology over the last few years, mainly for “last mile” applications, because FSO links provide the transmission capacity to overcome bandwidth bottlenecks between backbone optical fiber links and metropolitan concentrations of end users. Optical fiber has been traditionally deployed for the transmission of both digital and analog signals. While transmission techniques for analog radio frequency (RF) intensity-modulated signals over optical fibers is well-established, prior to the investigations presented in this dissertation, there is no report of research on the efficiency of FSO for transmission of analog signals in the technical literature. This dissertation research investigated the effectiveness of FSO to transport modulated RF analog signals and compares key performance measures against those of fiber optic links. In addition, a new method to setup temporary IS-95 CDMA microcells or permanent IS-95 CDMA macrocells using FSO was proposed and its viability investigated. Finally, a new transmission technique for transmitting multiple RF signals (channels) over a single FSO link using wavelength division multiplexing (WDM) technology for potential CATV applications was demonstrated.

Chapter 1

Introduction

Free-space optics (FSO) communication uses modulated optical beams, usually generated by laser sources or light emitting diodes (LEDs), to transmit data, voice, and multimedia through the atmosphere. There has been an exponential increase in the use of FSO technology over the last few years, mainly for "last mile" applications, because FSO links provide the transmission capacity to overcome bandwidth bottlenecks between the fiber and the metropolitan concentration of end users [1]. The desire to develop increased bandwidth Internet access has stimulated much of this growth and as a result, the major focus of most FSO research and development has been toward the transmission of digital signaling formats. Recently, FSO has provided the physical-layer transport infrastructure for the following digital applications [2-8]:

- Cellular telephony
- Voice-over-IP (VoIP)
- "Last Mile" applications
- Multiplexed voice and data
- Wireless redundant links
- LAN/ WAN extension
- Campus connectivity
- Deep space communications (under research and development)

Fiber optics has been traditionally deployed for transmission of both digital and analog signals. The transmission of analog radio frequency (RF) intensity-modulated signals over optical fibers is well-established [9, 17]. However, there is no report of research on the efficiency of FSO for transmission of analog signals in the technical literature. This dissertation investigates the effectiveness of FSO to transport modulated RF analog signals.

The *advantages* of transmitting modulated radio frequency (RF) signals over FSO links are as follows:

- FSO transmission links can be deployed *faster*, in some instances more *economically*, and provide a faster return on investment than optical fiber links.
- When evaluated with wireless RF links, FSO requires *no licensing*, provides better link *security* and much higher *immunity* to electromagnetic interference (EMI).
- FSO is highly *invulnerable* to interference from other sources of laser radiation [18-19].
- FSO can be applied for portable applications, e.g., providing high-bandwidth connectivity to movable radar dish antennas.
- FSO provides a practical transmission channel for transporting *IS-95 CDMA* signals to base stations from macro- and microcell sites and *can reduce the setup expenses* of temporary microcells deployed for particular events, e.g.,

sporting events, by reducing the need for installing directional microwave links or connecting cable [20-22].

- FSO introduces a viable transmission medium for the deployment of *CATV* links in metropolitan regions where installing new fiber infrastructure can be relatively expensive [23, 24].
- Generally, analog FSO can decrease the cost of transmission equipment as compared to a digital implementation.

The *objectives* of this dissertation research were as follows:

- The characterization of an end-to-end communication channel for transmission of modulated analog RF signal(s) over a FSO link, and the comparison of performance with an identical fiber optic link. The motivation for the comparison is the assurance that the RF photonic links provide the same attributes as conventional RF over optical links, but with lower cost, improved performance, better operating frequency, and lower complexity and size.
- The characterization of the forward and reverse channels established when a modulated analog IS-95 CDMA signal is transmitted over an FSO link. This study investigated the communication channels based on RF signal criteria and on user power criteria.

- The investigation of the simultaneous transportation of multiple RF signals over a single FSO link using wavelength division multiplexing (WDM) technology for potential CATV applications.

The evaluation and analysis of this dissertation for the key performance of RF photonic links were in terms of the same generally accepted criteria typically applied to conventional RF links. Typical performance criteria for conventional RF links include RF loss and frequency response, with no thought given to nonlinear distortion or additional noise unless the signal is amplified. In RF photonic links, additional noise generated by the laser source and the photodiode can degrade the Carrier-to-noise ratio (CNR), and nonlinearity of the modulation device can decrease the spurious free dynamic range. Thus, the important RF performance criteria for RF photonic links are:

- The RF gain and frequency response,
- The additional noise and CNR
- The spurious free dynamic range (SFDR).

The investigations of this dissertation have produced the following contributions:

- The demonstration of a new transmission technique for single-channel analog RF signals, e.g., a radar signal, using FSO technology [25]. This was the first reported study of its kind.
- An accurate comparison and analysis between the performance of FSO and fiber optic links, which is important in establishing the viability of FSO as an alternative to fiber in certain applications [26].
- The demonstration of a new transmission technique for multiple RF signals (channels), e.g., CATV signals, using FSO technology [27, 28].
- Proposed a new method to setup temporary IS-95 CDMA microcells or permanent IS-95 CDMA macrocells using FSO [29].

The remainder of the dissertation is organized as follows. Chapter 2 illustrates and analyzes the employed RF photonic technologies in FSO links. Chapter 3 provides the experimental study, supported with theoretical analysis, for the comparative study of the key performance of analog fiber-optic links versus FSO links. The transmission of cellular signals over FSO links to base stations from macro- and microcells is reported in Chapter 4. The deployment of *CATV* signals over free-space optical links is investigated in Chapter 5. Concluding remarks and suggestions for future research are given in Chapter 6.

Chapter 2

RF Photonic Technologies in Free-Space Optical Links

2.1 Introduction

With the widespread deployment of fiber optics, and more recently FSO, to serve the growing bandwidth demands of telecommunications networks, the predominant signal format has been digital. However, in many cases, it is more beneficial to transmit data in analog format instead of digital, because analog transmission eliminates the need for analog-digital-analog converters. Recent examples of analog applications include antenna remoting, hybrid optical/RF video distribution, and radar signal processing.

Figure 2.1 illustrates the basic components of an analog optical link and major sources of noise. The analog optical transmitter contains either an LED or a laser source modulated directly or externally. The simplest type of analog optical link is one that uses direct intensity modulation in which the optical signal generated from the transmitter is modulated by changing the optical amplitude in proportion to the RF signal level.

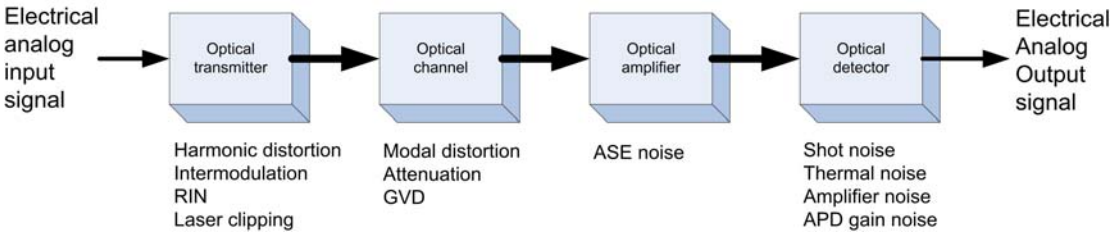

Figure 2.1 Basic Components of an analog optical link and major sources of noise [30]

The remainder of this chapter provides adequate explanations for the major RF photonic technologies used through this investigation. Also, this chapter explains the major noise sources and the impact of the existing nonlinear distortion on photonic link performance.

2.2 Fee-Space Optics (FSO)

FSO systems operate in the near infrared (IR) spectral range, from 850 to 1550 nm, which match frequencies around 200 THz [31]. These wavelengths are also utilized in fiber-optic communications so that industry standard transmitters and receivers can be used with FSO systems.

Frequencies above 300 GHz do not need a license from the Federal Communications Commission (FCC), contrary to most lower-frequency microwave systems, such as Local Multipoint Distribution System (LMDS). Simply, by installing the transceivers on both ends of the transmission path, FSO system can establish a point-to-point transmission link. The major condition for operating a FSO system is a visible line-of-

sight between the two networking positions. FSO systems utilize an optical beam to communicate; however, light cannot go through solid obstacles such as walls or trees [31]. A simple schematic of a free-space optics transmission system is shown in Figure 2.2.

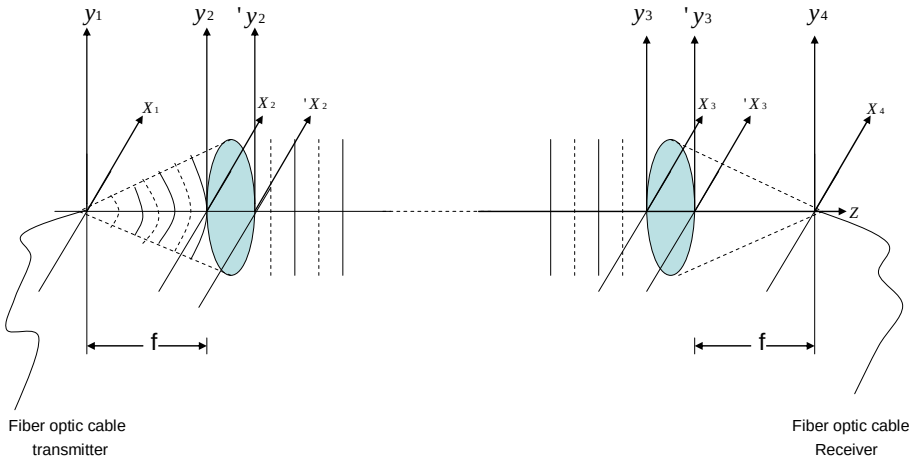

Figure 2.2 Schematic of a free-space optical transmission system

A FSO transmitter contains an optical transmitter and a telescope assembly which is designed to produce a beam with narrow divergence. Practically, the divergence of the optical beam connecting the transmission link varies between a few hundred microradians and a few milliradians. For instance, the diameter of the laser beam cross-section at 1 km is 1 m for a 1-milliradian beam divergence.

Employing a telescope, the receiver side of the FSO collects the transmitted optical beam and focuses it toward its photodetector via an optical fiber connecting the telescope with the photodetector. Pragmatically, the projected optical beam size at the receiving side is significantly larger than the size of the receiving telescope. Therefore, part of the transmitted optical beam is lost during the transmission process because of the divergence of the beam. The projected optical beam size can be several meters depending on the divergence of the beam, while the standard diameter of the receiving lens is more likely to be from 8 to 20 cm. This phenomenon is called *geometrical path loss*. Narrowing the transmitted optical beam decreases the amount of geometrical path loss. Another type of loss the optical FSO beam experiences during its propagation through the air is the *atmospheric path loss* which causes signal degradation and attenuation. Atmospheric loss is due to the following effects:

a. Absorption: the atoms and molecules in the air absorb some amount of light from the FSO optical beam, which leads to reduction of the signal power. The absorption effect is a function of the absorption strength of the particular particle and is also a function of the particle density.

b. Scattering: light scattering can dramatically affect the performance of the FSO system. In scattering, the optical energy loss is due to the redirection and redistribution of the FSO light in directions away from the receiver location.

c. Scintillation: the thermally induced changes in the refractive index of the air through the FSO path cause fluctuation of the received signal power and thus,

signal degradation.

d. Weather conditions: fog, rain, and snow are the main weather phenomena that can drastically affect the FSO system performance. Fog is the weather phenomenon that has the most advert effect on FSO performance because the size of the fog particles is near that of the employed FSO wavelength, which leads to a significant amount of light scattering. Rain has considerably less impact than fog, because the size of the rain drops is larger than the employed FSO wavelength. However, rain can significantly reduce the effective link distance of an operating FSO system. Snow flakes, which have a diversity of shape and size, can affect the FSO beam because of their ability to block the FSO path. With snow, scattering is not a major concern, because snow flake size is large when compared to the operating FSO wavelength.

All of these weather phenomena are time-varying. Table 2.1 illustrates the latest reported values of the atmospheric loss impacts on the FSO transmission with respect to the weather conditions. A significant number of previous investigations have looked at the affect of weather phenomena on FSO performance, resulting in models that allow prediction of signal degradation under varying conditions. Therefore, this dissertation has not focused on repeating such investigations.

Table 2.1 Visibility codes for weather conditions and precipitation [31]

Weather Condition	Precipitation		Amount	Visibility	dB Loss/km	Deployment Ranges (m)
Dense fog				0 m		
				50 m	-271.65	122 m
Thick fog				200 m	-59.57	490 m
Moderate fog	snow			500 m	-20.99	1087 m
Light fog	snow	Cloudburst	100	770 m	-12.65	1565 m
				1 km	-9.26	1493 m
Thin fog	snow	Heavy rain	25	1.9 km	-4.22	3238 m
				2 km	-3.96	3369 m
Haze	snow	Medium rain	12.5	2.8 km	-2.58	4331 m
				4 km	-1.62	5566 m
Light haze	snow	Light rain	2.5	5.9 km	-0.96	7146 m
				10 km	-0.44	9670 m
Clear	snow	Drizzle	0.25	18.1 km	-0.24	11468 m
				20 km	-0.22	11743 m
Very clear				23 km	-0.19	12112 m
				50 km	-0.06	13771 m

FSO systems provide data transport in a full duplex mode, i.e., information transmission and reception occurs simultaneously. Therefore, each FSO optical module typically includes a transceiver capable of full duplex operation.

In a digital transmission system, the transmitted signal is modulated by an electrical input signal that carries the actual network information. During the electrical-to-optical (E/O) conversion process, information is intensity modulated by the electrical input. This simple conversion operation separates the transmission path from the transported networking protocol. On the receiver side, a telescope collects the modulated optical signal and a photodetector converts the optical bit stream back into an electrical signal.

2.3 Analog Transmitters

The laser is the most important element in FSO links since it generates the coherent optical beam carrying the data. The laser frequency is about 200THz and the RF (10 KHz-300 MHz) or microwave (300 MHz- 300 GHz) waves can be modulated onto the laser beam either directly or externally. Recently, the electrical-optical devices most frequently used for implementing links are the in-plane diode laser for direct modulation and the Mach-Zehnder modulator for external modulation. The in-plane diode laser for direct modulation employs both a Fabry-Perot cavity and distributed feedback (DFB). Since in-plane diode lasers were used throughout this investigation, their structure and operating techniques will be discussed in detail in this chapter.

2.3.1 Direct Modulation

Direct modulation indicates that the modulation signal (RF signal) directly adjusts the intensity, or the amplitude, of the transmitted laser beam. As mentioned above, there are two major types of direct modulation devices; however, only DFB and another related device, the distributed Bragg reflector (DBR), are explained in this section.

2.3.1.1 Distributed Bragg Reflector

An ideal laser source generates a narrow spectrum at its output which generally indicates that the laser is single mode. Practically, there is no such laser source; however, manufacturers keep improving the production of their respective laser sources to be able to transmit the output spectrum as narrowly as possible.

From the laser source structure viewpoint, the frequency selective dielectric mirrors at the cleaved surfaces of the semiconductor ensure a single mode of radiation in the laser cavity. The mirrors in the distributed Bragg reflector, as shown in Figure 2.3 (a), were designed to operate as reflection type diffraction gratings. These mirrors have a periodic corrugated structure. Partially reflected waves can only construct a reflected wave when the wavelength satisfies the Bragg condition.

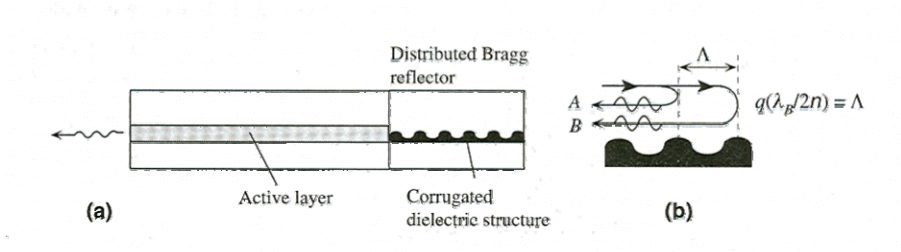

Figure 2.3 (a) Distributed Bragg reflection (DBR) laser theory. (b) Bragg condition [32].

As shown in Figure 2.3 (b), waves A and B reflected back interfere constructively when

$$q(\lambda_B / 2\eta) = \Lambda \qquad (2.1)$$

where λ_B is a Bragg wavelength, η is the refractive index, and $q = 1,2,...$ is an integer called the diffraction order. If q is not an integer, these waves interfere destructively.

2.3.1.2 Distributed Feedback Diode Laser

Normally, the crystal faces supply the required optical feedback into the cavity to construct the photon concentration. Figure 2.4 (a) illustrates the structure of distributed feedback (DFB) laser which contains a corrugated layer, named the guiding layer, located close to the active layer. The light wave produced in the active layer propagates parallel to the guiding layer which causes two counter propagating traveling waves to couple.

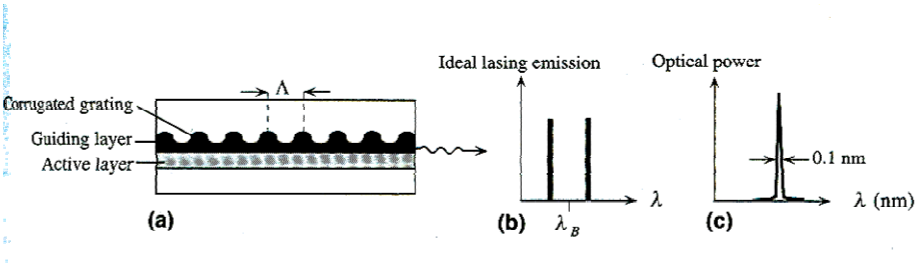

Figure 2.4 (a) Distributed feedback (DFB) laser structure. (b) Ideal lasing emission output. (c) Typical output spectrum from a DFB laser [32].

Traveling waves are reflected partially and periodically as they travel through the DFB structure. The left and right traveling waves can only coherently merge to construct a mode if their wavelength is correlated to the corrugation periodicity Λ . The permitted DFB modes are not precisely at Bragg wavelengths but are

symmetrically located around λ_B . Assuming λ_m is a permitted DFB lasing mode then

$$\lambda_m = \lambda_B \pm \frac{\lambda_B^2}{2\eta L}(m+1) \qquad (2.2)$$

where m = 1,2…. is a mode integer and L is the actual length of the diffraction grating (the length of the corrugation). A flawlessly symmetric device has two equally spaced modes located around λ_B as in Figure 2.4 (b). Practically, either expected asymmetry introduced by the fabrication process or asymmetry intentionally introduced leads to only one of the modes as shown in Figure 2.4 (c).

2.4 Photodetectors

An analog photodetector performs an optical-to-electrical conversion on the intensity modulated optical signal, whether this signal has been directly or externally modulated. A *pin* (p-intrinsic-n-type) photodiode produces an RF current proportional to the optical power at the frequency ω incident on the photodiode input $P_{ph,o}$. This notation indicates that

$$i_d = s_l P_{ph,o} \qquad (2.3)$$

where s_l is the slope efficiency for the utilized photodiode.

The *pin* photodiode structure consists of *p* and *n* layers separated by a very lightly *n*-doped intrinsic (*i*) layer. In standard operation, a suitably large reverse-bias voltage is

applied across the device so that the intrinsic region is completely depleted of carriers.

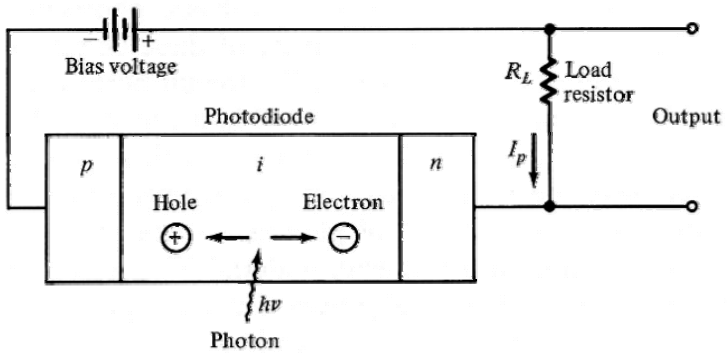

Figure 2.5 Schematic representation of a pin photodiode with an applied reverse bias [30]

When a photon with energy larger than the bandgap E_g is incident, it is absorbed to generate a free electron-hole pair (EHP), meaning an electron in the conduction band (CB) and a hole in the valence band (VB). Typically, the energy of the photon is such that photogeneration occurs in the depletion layer. The electric field in the depletion layer splits the EHP and forces them to drift in opposite directions until they arrive at the neutral areas, as depicted in Figure 2.5. Drifting carriers produce a current, called the photocurrent I_{ph}, in the external circuit that supplies the electrical signal [30]. The photocurrent remains for the duration needed for the electron and hole to travel through the depletion layer (W) and arrive at the neutral areas. When the drifting hole arrives at the neutral p-area it recombines with an electron incoming from the p-side from the negative electrode, meaning from the battery [30]. Also, when the drifting electron arrives at the neutral n-side, an electron leaves the n-side into the electrode

(battery). The photocurrent I_{ph} depends on the number of EHPs photogenerated and the drift velocities of the carriers while they are passing the depletion layer. Drift velocity is proportional to the applied field up to a scattering-limited value, i.e., the saturation drift velocity, as shown in Figure 2.6.

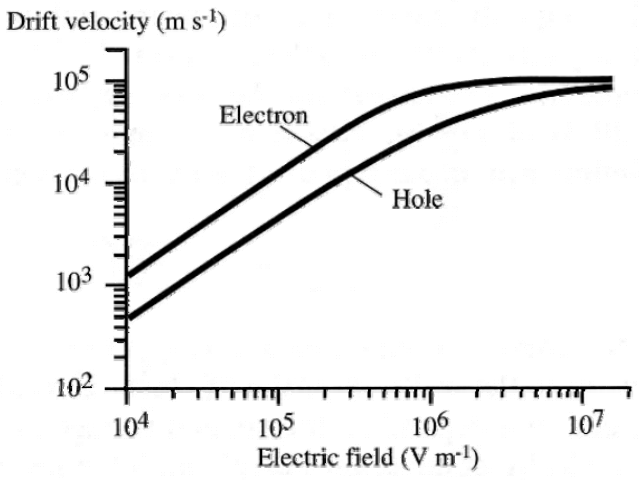

Figure 2.6 Drift velocity vs. electric field for holes and electrons in Si.[32]

2.5 Sources of Noise

Figure 2.7 illustrates the mechanism used to generate an optical signal using an analog optical transmitter. The drive current through the optical source is the combination of both the fixed bias current and a time-varying sinusoid. As a result, the envelope of the output optical power $P_{l,o}$ has the same shape as the input drive current. Mathematically, the modulation is defined by

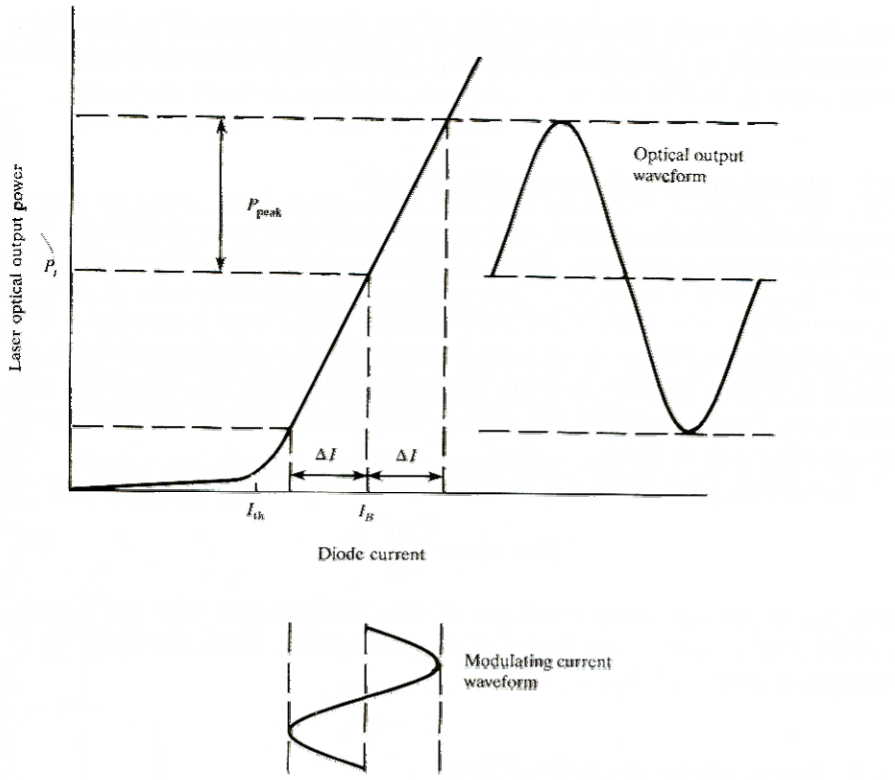

Figure 2.7 The response of laser diode to analog modulation signal [30]

$$P_{l,o} = P_{l,om}.\{1 + m.s(t)\} \tag{2.4}$$

where $P_{l,om}$ is the optical output power at the bias current level and m is the modulation index.

There are three key statistically independent sources of noise in RF photonic links [33, 34]:

2.5.1 Thermal Noise

The thermal noise is caused by the thermally induced electron movement in the conductors. The mean-squared current of the thermal noise is given by

$$\left\langle i^2_{Thermal\ Noise} \right\rangle = \frac{4kTB}{R} \qquad (2.5)$$

where k is Boltzmann's constant, T is the absolute temperature in degrees Kelvin, B is the noise bandwidth in Hz, and R is the resistance creating the noise in Ohms.

2.5.2 Shot Noise

The Shot noise is generated by the photodiode which produces an electrical current proportional to the optical signal at the input. When an external laser modulator is employed, the shot noise is the dominant noise source. The mean-squared current due to shot noise is given by

$$\left\langle i^2_{Shot\ Noise} \right\rangle = 2e\left\langle I_d \right\rangle B \qquad (2.6)$$

where e is the electron charge, I_d is the dark leakage current in Amps, and B is the noise bandwidth in Hz.

2.5.3 Relative Intensity Noise RIN

The Relative Intensity Noise (RIN) is caused by spontaneous emission in the laser source. These variations of laser intensity at the laser transmitter output

can have impact at the photodiode output after being converted to electrical current. The mean-squared noise current is given by

$$\left\langle i_{RIN}^2 \right\rangle = \frac{\left\langle I_d \right\rangle^2}{2} 10^{RIN/10} B \tag{2.7}$$

where *RIN* is the optical noise power, I_d is the dark leakage current, and B is the noise bandwidth. When a directly modulated laser transmitter is employed, the RIN is dominant over all other noise sources throughout the RF photonic link.

2.6 Noise Figure

Noise figure illustrates the relationship between the noise present at the output of the RF photonic link n_{out} and the noise generated at the input of the link n_{in} at a standard temperature of 290 K. Noise figure NF is defined as,

$$NF = 10\log\left(\frac{s_{in}/n_{in}}{s_{out}/n_{out}}\right) = 10\log\left(\frac{n_{out}}{g_{rf} n_{in}}\right) \tag{2.8}$$

where $n_{in} = n_{thermal\,noise} = kTB$, T=290 K, s_{in} and s_{out} are the RF signal power at the input and the output of the RF photonic link at frequency ω.

When there is no noise introduced through the link, the noise figure NF equals 0 dB. The output power and the output noise power can be expressed as follows:

$$s_{out} = g_{rf} s_{in}, \tag{2.9}$$

$$n_{out} = g_{rf} n_{in} + n_{extra}, \tag{2.10}$$

where n_{extra} is the additional noise added through the RF photonic link. Rewriting Eq. (2.8) as

$$NF = 10\log\left(1 + \frac{n_{extra}}{g_{rf} n_{in}}\right) \tag{2.11}$$

As shown from Eq. (2.11), NF is usually employed to identify the noise property of any RF components through any RF photonic link.

2.7 Distortion in RF Photonic Links

Up to this section, only linear SNR or gain for an optical link has been examined. Typically, the gain correlates the RF power when the fundamental frequency ω reaches the load R_L with the input RF power at the same frequency ω. On the other hand, careful scrutiny of the output shows that it will contain not only the signal at the fundamental signal frequency ω but also at frequencies that are harmonically correlated to the fundamental. More precisely, there will be nonlinear distortion for the fundamental signal frequency ω. The harmonic signal frequencies need to be smaller than the noise floor if a communications link is employed in linear applications. Dynamic range measurements indicate the range of the RF input power in which no distortion of the output signal occurs due to the effects of harmonic distortion. Nonlinear devices built-in the analog transmitters and receivers are the

major causes of distortion in an optical link, particularly the analog modulators [10]. Distortion is a key link parameter in certain distribution systems that convey multiple carriers, such as CATV applications [27]. However, it has minor importance in distribution systems that carry one single frequency, such as radar applications. Contrary to the noise, distortion is a deterministic phenomenon which can be defined for any link that includes nonlinear devices. Also, distortion is an input signal dependent phenomenon which indicates the absence of distortion for any link with the absence of the input signal. On the contrary, noise is present in the link even with the absence of the input signal.

As explained earlier in this chapter, the i_{TLoad} consists of a DC bias photocurrent, I_{BLoad}, in addition to the RF and distortion signals. Mathematically, the distortion can be investigated starting from the link input voltage to the link output current, where the link output photocurrent is correlated with the link input voltage through the link transfer function h :

$$i_{TLoad}(t) = h[V_B + v_{rf}] \tag{2.12}$$

Analyzing Eq. (2.12) according to small signal approximation indicates the ability of approximating the transfer function h using a Taylor series expansion which substitutes the non-linear transfer function h with an infinite sum of derivatives of the function with respect to the input voltage at a given value, V_B.

$$i_{TLoad} = h(V_B) + v_{rf}\left.\frac{\partial h}{\partial V}\right|_{V=V_B} + \frac{v_{rf}^2}{2!}\left.\frac{\partial^2 h}{V^2}\right|_{V=V_B} + \frac{v_{rf}^3}{3!}\left.\frac{\partial^3 h}{\partial V^3}\right|_{V=V_B} + \frac{v_{rf}^k}{k!}\left.\frac{\partial^k h}{\partial V^k}\right|_{V=V_B} + ...$$

$$i_{TLoad} = I_{BLoad} + h_1 v_{rf} + h_2 v_{rf}^2 + h_3 v_{rf}^3 + ... + h_k v_{rf}^k + ...$$

where,

$$h_k = \frac{1}{k!}\left.\frac{\partial^k h}{\partial V^k}\right|_{V=V_B}$$

Assuming that the RF modulation signal is a pure sinusoid, $V = V_B + v_m \cos\omega t$. Using a Taylor series expansion to express the output signal of a nonlinear link indicates the following:

$v_{rf(t)} = v_m \cos\omega t$,

$v_{rf}^2 = \frac{1}{2}(v_m)^2(1+\cos 2\omega t)$,

$v_{rf}^3 = \frac{1}{4}(v_m)^3(3\cos\omega t + \cos 3\omega t)$,

$v_{rf}^4 = \frac{1}{8}(v_m)^4(\frac{6}{2} + 4\cos 2\omega t + \cos 4\omega t)$,

Thus, the h_k term indicates the kth harmonic distortion at the frequency kw. Also, it indicates the $(k-2)\omega t,(k-4)\omega t,....,(k-2m)\omega t,....$ as lower frequency terms. As a result, i_{TLoad} expression can be rewritten as

$$\begin{aligned} i_{TLoad} &= I_{BLoad} + \frac{1}{2}h_2(v_m)^2 + \frac{6}{16}h_4(v_m)^4 + ... \\ &+ \left[h_1 v_m + \frac{3}{4}h_3(v_m)^3 + \frac{10}{16}h_5(v_m)^5 + ... \right]\cos\omega t \\ &+ \left[\frac{1}{2}h_2(v_m)^2 + \frac{4}{8}h_4(v_m)^4 + ... \right]\cos 2\omega t \\ &+ \left[\frac{1}{4}h_3(v_m)^3 + \frac{5}{16}h_5(v_m)^5 + ... \right]\cos 3\omega t + ... \qquad (2.13) \end{aligned}$$

$$= I_{BLoad} + i_{Load}\cos\omega t + i_{2Load}\cos 2\omega t + i_{3Load}\cos 3\omega t + ... \qquad (2.14)$$

It is important to recognize these terms presented in Eq. (2.13). The fundamental frequency magnitude is much larger than the 2nd harmonic magnitude, which is larger than the 3rd harmonic magnitude, etc.

Clearly, the harmonic signals have the following orders with their respective frequencies:

Second order harmonic distortion (2HM): 2ω;

Third order harmonic distortion (3HM): 3ω.

There is another and more practical method for measuring the dynamic range. When the link input is supplied by two closely spaced sinusoids of equal magnitude, it characterizes a distortion signal. Using the same previous mathematical technique leads to a comprehensive analysis of the distortion signals for the link. Assuming

$$v_{rf}(t) = v_m(\cos\omega_1 t + \cos\omega_2 t)$$

where $\omega_1 \approx \omega_2$ yields a variety of combined frequency terms plus the harmonic signals for each sinusoid:

$$i_{TLoad} = h(V_B) + v_{rf}\left.\frac{\partial h}{\partial V}\right|_{V=V_B} + \frac{v_{rf}^2}{2!}\left.\frac{\partial^2 h}{V^2}\right|_{V=V_B} + \frac{v_{rf}^3}{3!}\left.\frac{\partial^3 h}{\partial V^3}\right|_{V=V_B} + \frac{v_{rf}^k}{k!}\left.\frac{\partial^k h}{\partial V^k}\right|_{V=V_B} + ...$$

$$i_{TLoad} = I_{BLoad} + h_1 v_{rf} + h_2 v_{rf}^2 + h_3 v_{rf}^3 + ... + h_k v_{rf}^k + ...$$

where,

$$h_k = \frac{1}{k!}\left.\frac{\partial^k h}{\partial V^k}\right|_{V=V_B}$$

Assuming that the RF modulation signal is a purely sinusoidal one, $V = V_B + v_m \cos\omega t$. Using the Taylor series expansion to express the output signal of a nonlinear link indicates the following:

$v_{rf}(t) = v_m(\cos\omega_1 t + \cos\omega_2 t)$,

$$v_{rf}^2 = (v_m)^2\left[\frac{1}{2}(1+\cos(2\omega_1 t)) + \frac{1}{2}(1+\cos(2\omega_2 t)) + \cos(\omega_1+\omega_2)t + \cos(\omega_1-\omega_2)t\right],$$

$$v_{rf}^3 = (v_m)^3 \left[\begin{array}{l} \frac{7}{4}(\cos(\omega_1 t) + \cos(\omega_2 t)) + \frac{1}{4}\left(\cos(3\omega_1 t) + \cos(3\omega_2 t)\right) + \\ \frac{3}{4}\left(\cos(2\omega_1 + \omega_2)t + \cos(2\omega_2 + \omega_1)t + \cos(2\omega_1 - \omega_2)t + \cos(2\omega_2 - \omega_1)t \right. \end{array} \right]$$

$$\begin{array}{l} i_{TLoad} = I_{BLoad} + v_m(\cos\omega_1 t + \cos\omega_2 t) + \\ h_2 v_m^2 \left[\frac{1}{2}\left(1 + \cos(2\omega_1 t) + \frac{1}{2}\left(1 + \cos(2\omega_2 t) + \cos(\omega_1 + \omega_2)t + \cos(\omega_1 - \omega_2)t \right) \right) \right] + \\ h_3 v_m^3 \left[\begin{array}{l} \frac{7}{4}(\cos(\omega_1 t) + \cos(\omega_2 t)) + \frac{1}{4}\left(\cos(3\omega_1 t) + \cos(3\omega_2 t)\right) + \\ \frac{3}{4}\left(\cos(2\omega_1 + \omega_2)t + \cos(2\omega_2 + \omega_1)t + \cos(2\omega_1 - \omega_2)t + \cos(2\omega_2 - \omega_1)t \right. \end{array} \right] \end{array} \quad (2.15)$$

These resulting distortion signals are referred as intermodulation distortions which have the following orders with their respective frequencies:

Second order intermodulation distortion (2IM): $\omega_1 \pm \omega_2$, $2\omega_1$, $2\omega_2$;

Third order intermodulation distortion (3IM): $2\omega_1 \pm \omega_2$, $2\omega_2 \pm \omega_1$, $3\omega_1$, $3\omega_2$.

Figure 2.8 illustrates the graphical demonstration of the free dynamic range (FDR) in output power versus input power plot.

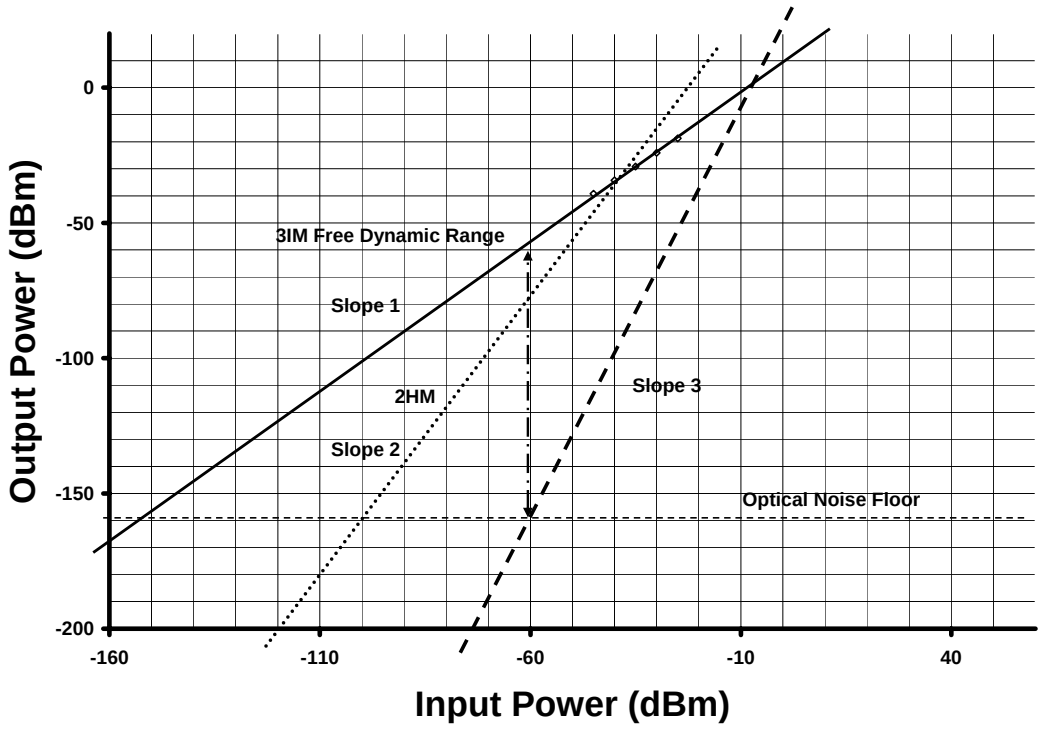

Figure 2.8 Graphical demonstration of free dynamic range (FDR) in a output power vs. input power

For narrowband systems, most 2IM and 3IM will be filtered and eliminated except the two 3IM spaced close to the fundamental frequency.

2.8 Summary

Essentially, FSO system components are made of a light source, transmitting telescope to direct and focus the light, receiving telescope to deliver the light, and electrical-optical electronics to manage conversions of electrical and optical communications. The required technologies are similar to that of conventional fiber-

optics except that some unique components required replacing the fiber-optic transmission medium with that of free-space. This chapter developed the small-signal relationships between the RF and optical parameters for the most common electrical/optical devices used throughout this investigation.

Chapter 3

A Comparative Study of the Performance of Analog Fiber-Optic Links versus Free-Space Optical Links

3.1 Introduction

Free-space optics (FSO) provides bi-directional data transmission through the atmosphere between two aligned transceivers using high-power, modulated infrared laser beams. Fiber optics has been conventionally used for transmission of both digital and analog signals. This chapter investigates the efficiency of FSO to transport modulated radio frequency (RF) analog signals and compare it with that of fiber optics in similar surroundings. This transmission of RF analog signals over FSO links can be implemented for portable applications, e.g., cable free interconnection of movable radar dish antennas with their base stations.

The remainder of the chapter is organized as follows. Section 3.2 describes the experimental setup to transmit modulated RF signals over fiber optics and FSO. The experimental results with related theoretical studies are reported in Section 3.3, which includes measurements of optical power, transmission response, reflection response, group delay, carrier-to-noise ratio (CNR), and dynamic range for RF analog signal transmission over both fiber optic and FSO links.

3.2. Experimental Setup

Figure 3.1 shows the experimental setup used in transmission response, reflection response, and group delay measurements for both fiber optic and FSO links. An Aurora AT3510 analog laser transmitter, with an ITU grid compliant output wavelength of 1552.524 nm, was fiber connected to either a Dominion Lasercom DAViD® FSO telescope assembly, or a 3 m optical fiber. In the first instance, the transmitting telescope was aligned line-of-sight with a similar receiving telescope that was nearly 3 m away. The gap between both telescopes was small, but sufficient to characterize the main performance measures of the channel between the optical transmitter and receiver. Deployed FSO systems will experience atmospheric loss, as explained in the Chapter 2, but such loss can be effectively modeled. The receiving telescope was fiber-connected to an Aurora AR4001 analog receiver. In the second instance, the 3 m optical fiber was coupled to the same fiber jumper that connected the receiving telescope to the AR4001, consequently matching the same jumper and connector losses throughout the analog communications channel.

The RF frequency range of operation for the transmitter and receiver was from 46 MHz to 870 MHz. The RF input signal to the transmitter was generated by an Agilent 8712ET RF vector network analyzer. The RF output signal from the analog receiver was fed back into the network analyzer. For measurements, a built-in RF amplifier inside the analog receiver and an Aurora OA4444T-42 RF amplifier were

connected between the receiver output and the input of the network analyzer, thus providing RF signal gain.

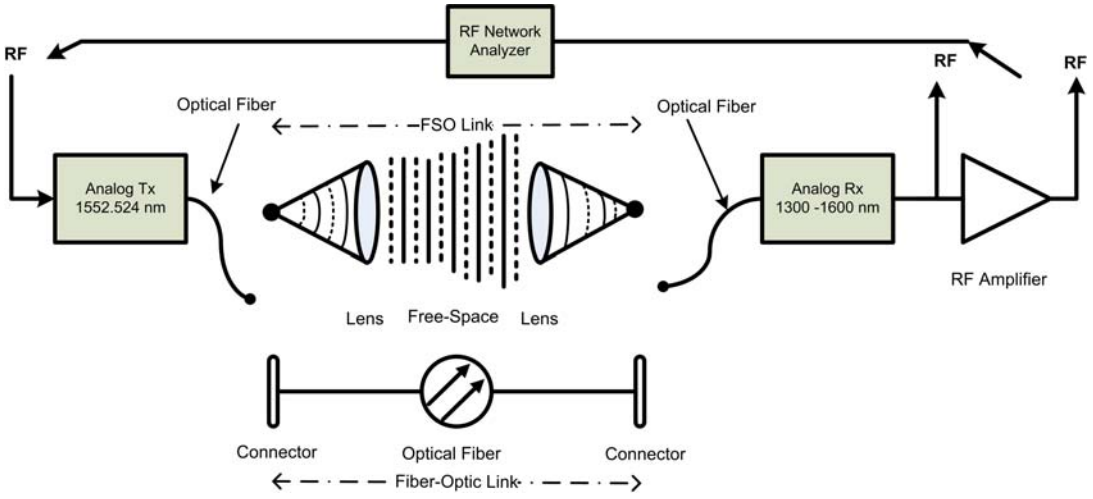

Figure 3.1 The experimental setup for measuring transmission response, reflection response, and group delay.

Figure 3.2 shows the experimental setup used in the CNR measurements. Comparing with Figure 3.1, note that the only major difference between these experimental setups is that, for the CNR measurements, the vector network analyzer has been substituted by a Rohde & Schwarz SMHU signal generator to provide RF signal to the transmitter. A Tektronix WCA280A wireless communication analyzer was connected for RF output signal measurements. CNR measurements were made with and without the RF amplifier.

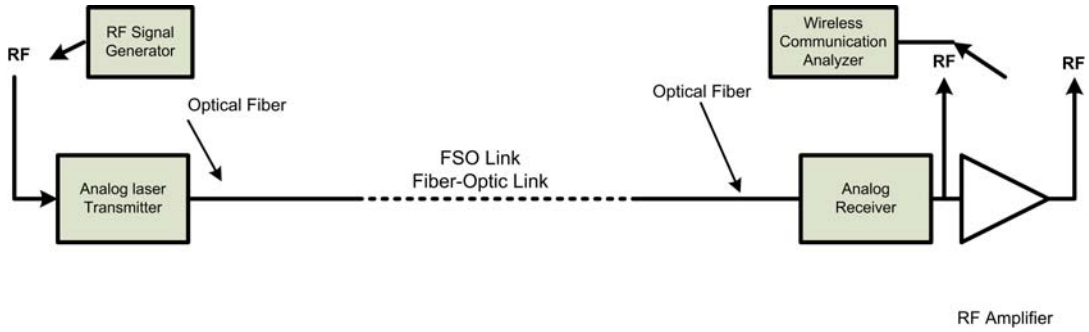

Figure 3.2 The experimental setup for measuring carrier-to-noise ratio (CNR).

For the dynamic range measurements, the only major change in the setup (see Figure 3.3) from Figure 3.1 was that, upon removal of the vector network analyzer, the Rohde & Schwarz SMHU and Agilent 8642A signal generators were linked to the transmitter input to inject the composite RF input signals.

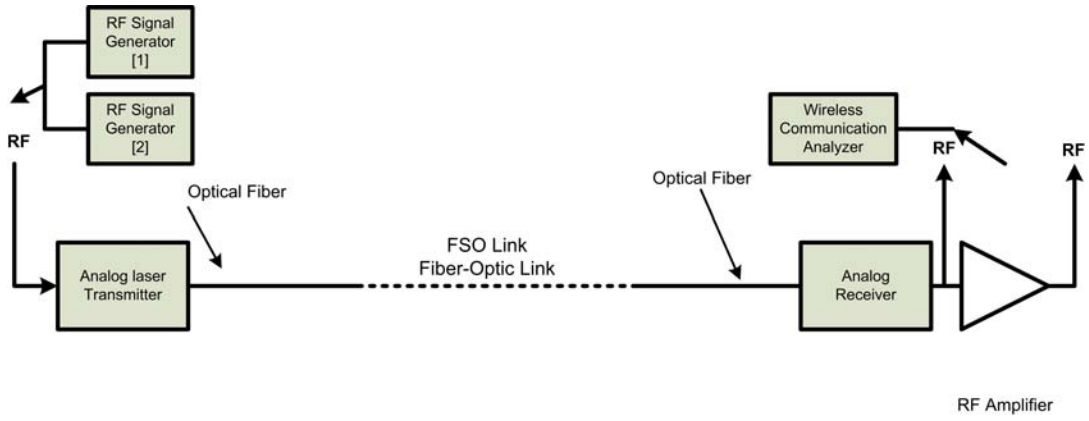

Figure 3.3 The experimental setup for measuring the dynamic range.

The operating wavelength of 1552.524 nm is well matched with most commercial FSO systems that operate at or near 1550 nm. From a laser safety perspective, higher

output powers can be employed since the human eye is less susceptible to damage at this wavelength. With these higher output powers, the FSO links can be extended and better able to operate under degraded meteorological conditions, e.g., fog and rain [35].

3.3 Experimental Results and Analysis

In this section, experimental measurements and analysis of optical power, transmission and reflection response, group delay, CNR, and dynamic range are reported. These studies comprehensively characterize the communication channels for both fiber optic and FSO links.

3.3.1 Optical Power Measurements and Analysis

Examination of the analog optical links must be evaluated based upon optical and RF criteria. This subsection presents a complete study of the optical criteria, delivering the results of the optical measurements for both fiber-optic and FSO links and demonstrates the existing sources of optical loss that influence the optical power during its transmission through both links. The RF criteria are investigated in detail in the upcoming subsections.

From the optical point of view, the amplitude of the RF intensity modulated optical signal is much less than the intensity of the unmodulated optical carrier. As a result, the link can be characterized using the small signal approximation. Beginning with the analog fiber-optic link, the peak optical power and output wavelength of the analog laser transmitter were captured using an Advantest Q8384 optical spectrum analyzer. The resulting measurements show that the peak power and wavelength at the output of the analog transmitter were 9.49 dBm and 1552.530 nm, respectively. These values are shown in the lower table of Figure 3.4.

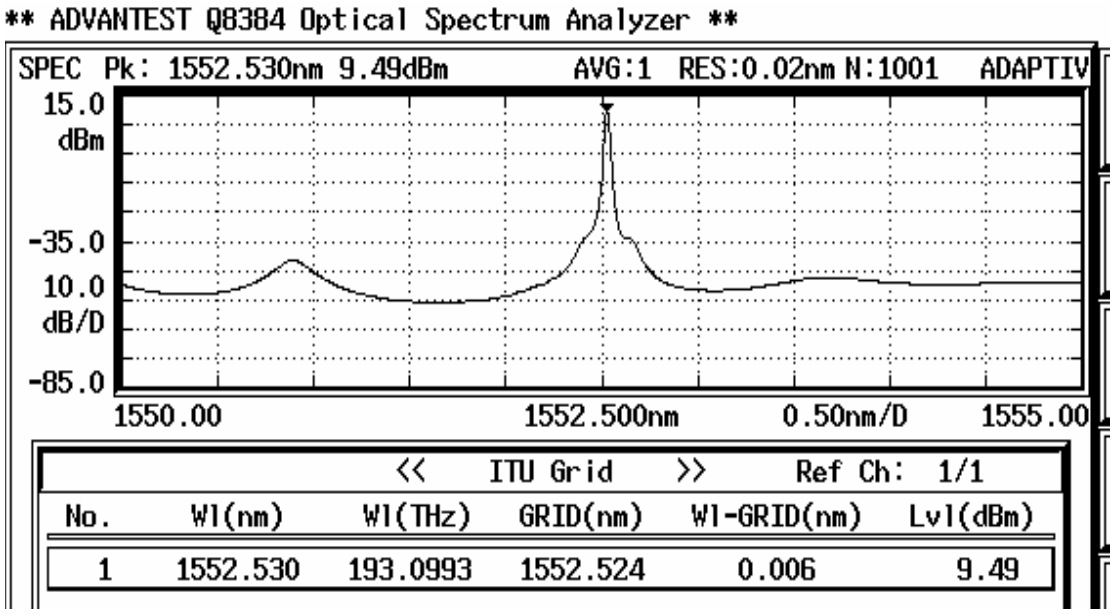

Figure 3.4 A screen capture from the Advantest Q8384 optical spectrum analyzer illustrating the results of peak power and output wavelength measurements at the output of the analog laser transmitter.

These measurements were repeated at the input of the analog receiver, indicating a peak power and output wavelength of 6.05 dBm and 1552.535 nm, respectively. These values are shown in the lower table of Figure 3.5. The sensitivity of the photodiode inside the analog receiver is nearby 0 dBm, which indicates the existence of extra power margin that can be employed to extend the link distance.

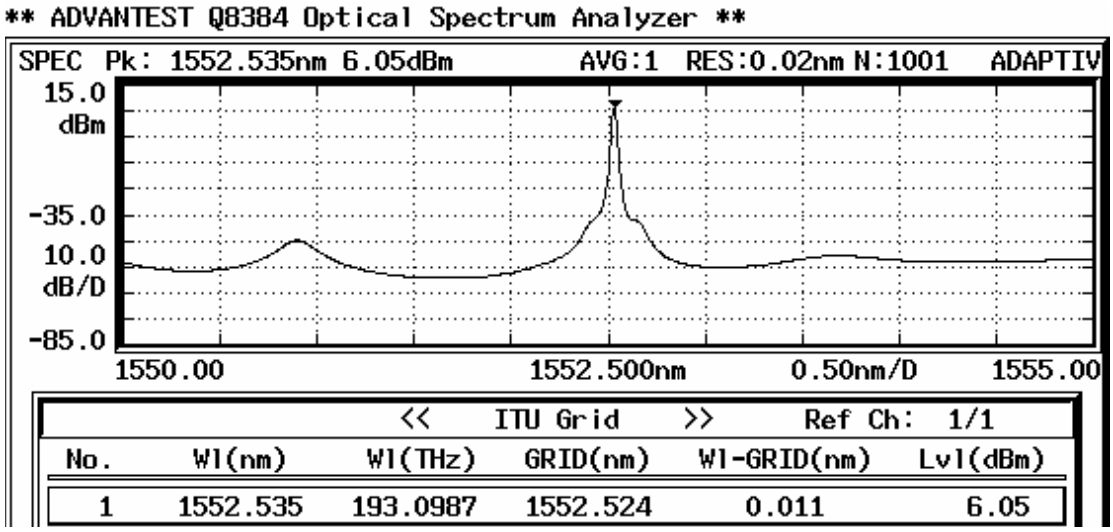

Figure 3.5 A screen capture from the Advantest Q8384 optical spectrum analyzer illustrating the results of peak power and output wavelength measurements at the input of the analog receiver.

Clearly, there is a loss in the signal power of approximately 3.45 dB. The sources of loss are connectors, jumpers, and attenuation taking place during the transmission through the optical fiber. Since the total length of the fiber path from the transmitter to the receiver is eleven meters, including the fiber jumpers connecting the transmitter and the receiver with the main fiber span, the optical signal experiences little

attenuation. Therefore, the major sources of loss in this instance were the connectors and jumpers - nearly 3 dB.

Injecting the same optical signal measured at the output of the analog laser transmitter, as shown in Figure 3.4, to the analog FSO link illustrates the optical difference between both fiber and FSO links. Using the Advantest Q8384 optical spectrum analyzer, a peak power of -4.21 dBm and output wavelength of 1552.530 nm was captured at the input of the analog receiver. These values are shown in the lower table of Figure 3.6.

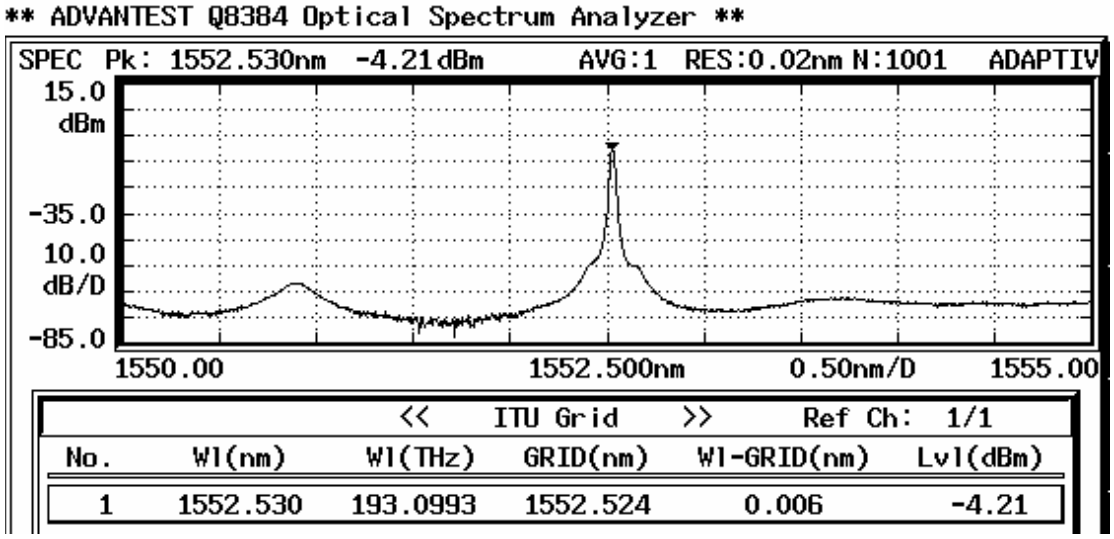

Figure 3.6 A screen capture from the Advantest Q8384 optical spectrum analyzer illustrating the results of peak power and output wavelength measurements at the input of the analog receiver.

Clearly, there is a loss in signal power of nearly 13.70 dB. Major sources of optical loss are insertion, lens, geometric, and atmospheric losses. Figure 3.7 shows the sources of power loss throughout the FSO link.

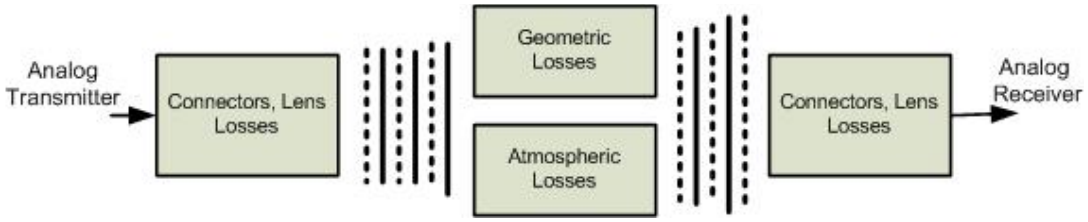

Figure 3.7 Sources of loss in FSO link.

Geometrical losses arise due to the divergence of the optical beam. These losses can be computed using the following formula [9]

$$\frac{A_R}{A_B} = \left(\frac{D_R}{D_T + 100 * d * \theta} \right)^2 \tag{3.1}$$

where D_T and D_R are the diameters of the transmitting and receiving lenses measured in cm, both 5 cm in this instance. The space gap between the FSO transmitter and receiver is d, measured in km, d = 0.003 km in this instance. θ is the divergence of the transmitted laser beam in mrad, θ = 2 mrad in this instance. Using (1), the calculated geometrical loss for this experimental setup is nearly 1 dB. This loss is

low because the distance between the FSO transmitter and receiver is only 3 m. Therefore, it does not add considerably to the total loss of 13.70 dB.

Atmospheric losses are due to absorption, scattering, scintillation, and weather conditions. Since these experiments were performed in a laboratory surrounding over a short distance, atmospheric losses are small. The connectors and FSO telescope assemblies at the transmitting and receiving ends are responsible for a large amount of insertion loss, nearly 12.70 dB in this instance. Typical insertion losses for industrial FSO links are around 4 dB. The insertion loss was high in these experiments because the FSO telescope assemblies and connectors were not optimally produced to interface the analog transmitter and receiver. Under typical operation, the Dominion Lasercom DAViD® FSO system presents an optical power at the transmitter output of around 20 dBm (100 mW), to overcome the propagation loss plus the insertion losses.

3.3.2 Transmission Response Measurements and Analysis

RF transmission response measurements determine the amount of loss, or gain, in a communications link with respect to the signal frequency. The RF transmission response of a RF photonic link is frequency dependent. There are three main reasons of frequency dependence: 1) the laser source, directly modulated or externally modulated, may have frequency dependent features, 2) the voltage or current reaching

the analog modulator may have frequency dependent response due to the electrical characteristics of the input circuit, and 3) the analog receiver, including its photodiode, may have frequency dependent characteristics. Any signal attenuation or gain due to the communications link will manifest itself in the transmission response measurement. The vector network analyzer plots the RF output measurement trace using

$$Transmission(dB) = 10\log\left(\frac{p_{trans}}{P_{inc}}\right) \tag{3.2}$$

where P_{trans} is the RF power measured at the output of the receiver and P_{inc} is the RF power measured at the input to the laser transmitter. Results of the transmission response measurements, with and without the RF amplifier included, for the fiber optic link are shown in Figure 3.8. There is a built in RF amplifier linked to the output of the photodiode inside the analog receiver, which produces up to 23 dB of gain depending on the operating frequency. As a result, the acquired gain can compensate the loss generated by the optical/RF conversion stage in the receiver. As mentioned before, the received optical power at the input of the photodiode is still greater than the sensitivity, which cancels the impact of the attenuation through the optical fiber.

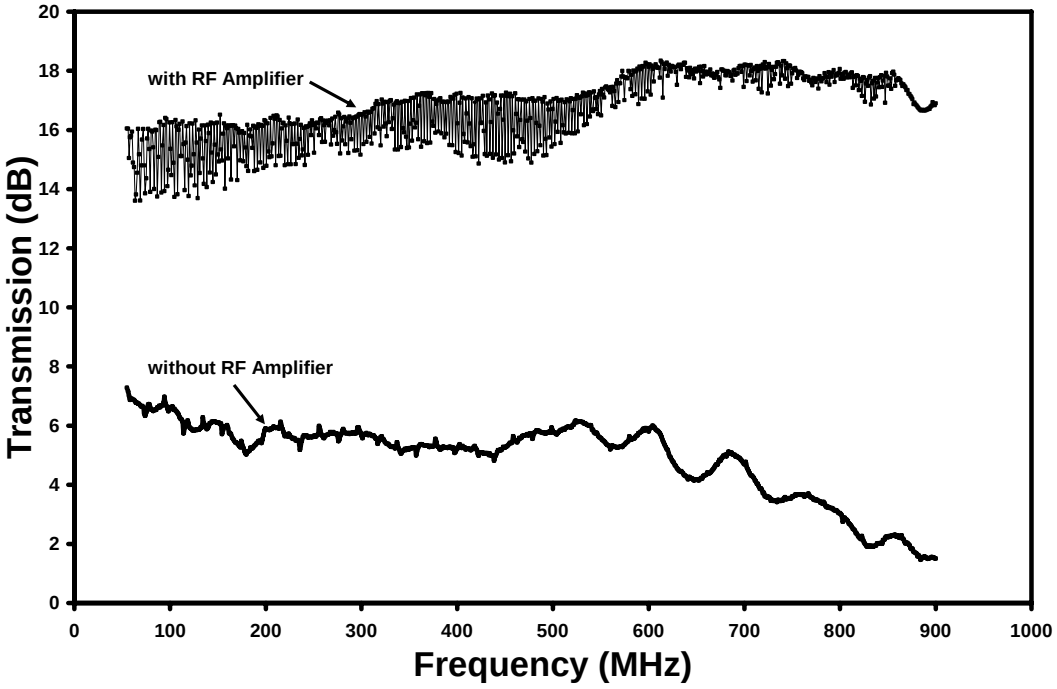

Figure 3.8 Transmission response measurements for fiber-optic link.

Without the RF amplifier, the transmission response varied from 1.50 dB to 7.28 dB over the frequency range of 55-870 MHz. These measurements compare positively with the -20 to -50 dB loss reported as typical for analog fiber optic links [36]. With the RF amplifier, the transmission response (gain) varied from approximately 13.69 dB to 18.34 dB over the same frequency range.

The results of the transmission response measurements for the FSO link, with and without the RF amplifier included, are shown in Figure 3.9. Transmission response without the RF amplifier varied between -12.11 dB and -19.03 dB over the frequency range 55-870 MHz, while the transmission response with the RF amplifier varied between 7.65 dB and 13.53 dB over the same frequency range. The figure illustrates a

relatively smooth response over the frequency range of 55-870 MHz. These measurements compare favorably with the previously reported measurements in this study through the fiber-optic link. Insertion of the RF amplifier generated sufficient gain to overcome the FSO link losses, thus allowing the FSO signal to travel farther distances.

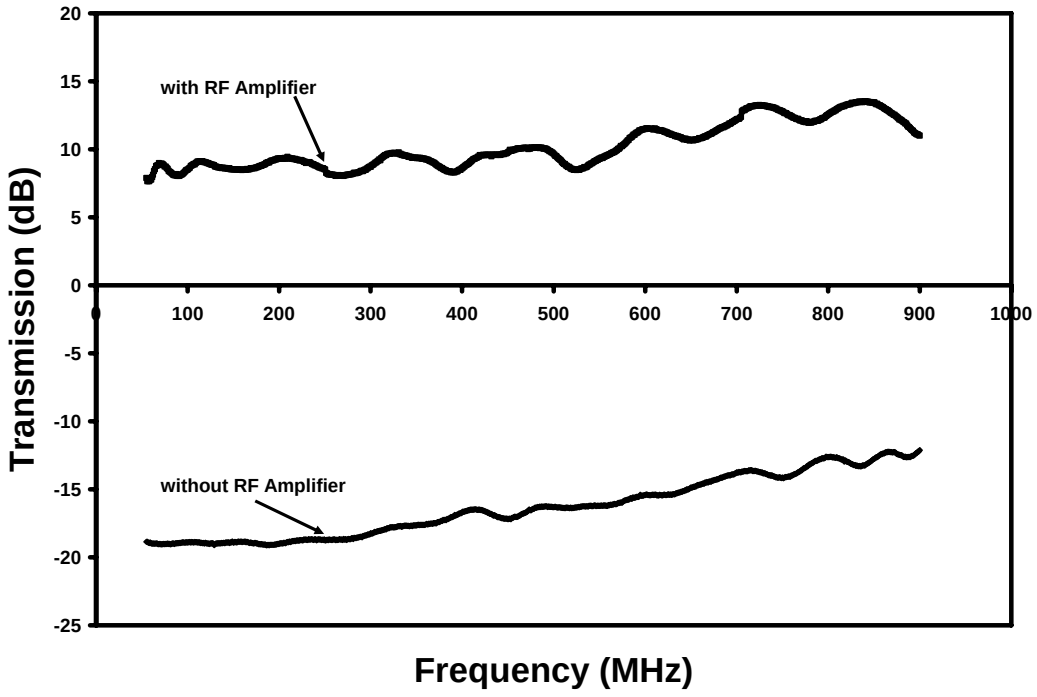

Figure 3.9 Transmission response measurements for free-space optic link.

Analog optical links exhibit two types of losses, optical and RF losses. Assume L_o is the optical loss that the incident analog signals experienced between the modulation and photodectection devices. This quantity includes the propagation loss of the free-

space or the optical fiber, plus the coupling loss to and from the FSO telescopes or the fiber span. With the absence of any optical amplification stage through the link, the range of the optical loss is defined as $0 \le L_o \le 1$. The optical transmitted power at the end side of the optical link can be expressed as:

$$P_{transmitted,o} = L_o P_{incident,o} \tag{3.3}$$

where $P_{incident,o}$ is the rms magnitude of the time varying optical power at frequency ω in the optical link immediately after the modulation device. $P_{transmitted,o}$ is the rms magnitude of the optical power at frequency ω incident on the detector.

Applying these notations:

1. $P_{incident,o}$ is proportional to the current or voltage of the RF input. Therefore, $P^2_{incident,o}$ is proportional to $P_{incident}$.
2. The RF current at the output of the link is proportional to $P_{transmitted,o}$. Therefore, the RF power is proportional to the square of the photocurrent, which indicates that $P^2_{transmitted,o}$ is proportional to $P_{transmitted}$.

Substituting these notations into Eq. (3.3) and Eq. (3.4) leads to Eq. (3.5)

$$Transmission = \frac{P_{transmitted}}{P_{incident}} \tag{3.4}$$

$$Transmission = \left(\frac{P^2_{incident,o}}{P_{incident}} \right) L_o^2 \left(\frac{P_{transmitted}}{P^2_{transmitted,o}} \right) \tag{3.5}$$

Asserting this equation in terms of dB shows that

$$Transmission\,(dB) = 10\log\left(\frac{P_{incident,o}^2}{P_{incident}}\right) + 20\log(L_o) + 10\log\left(\frac{P_{transmitted}}{P_{transmitted,o}^2}\right) \qquad (3.6)$$

Clearly, since L_o is squared in Eq. (3.5), when the log is taken in Eq. (3.6), it has double impact on the overall RF loss. Assuming $L_o = 1$, i.e., the optical path is lossless, provides the intrinsic link gain only in terms of the modulation and photodetection device parameters.

$$Transmission = \left(\frac{s_t^2}{R_L + R_{Match}}\right)\left(\eta_r^2 R_{Load}\right) \qquad (3.7)$$

As explained in Chapter 2, a PIN photodetector was used at the receiver side throughout this research. Assume that the resistive impedance of the RF source matches the laser impedance.

When $R_L + R_{Match} = R_{Load}$ as shown in Figure 3.10, this simplifies the equation of the link gain to the product of a square of the slope efficiency and responsivity.

$$Transmission = \eta_r^2 . s_t^2 \qquad (3.8)$$

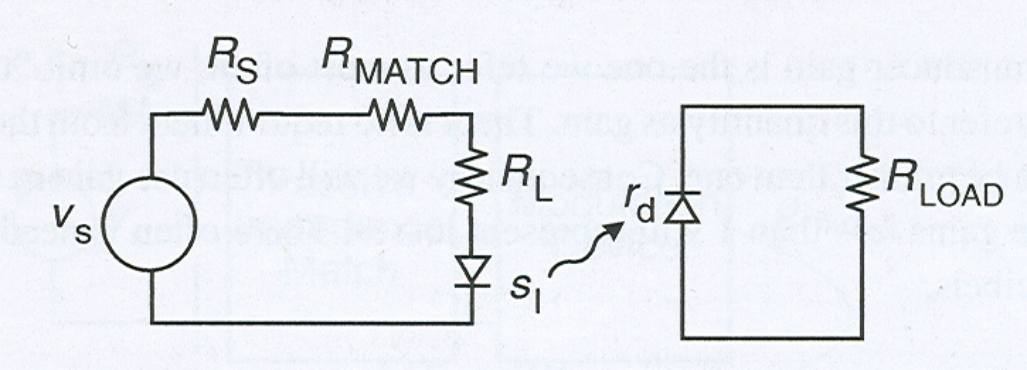

Figure 3.10 Direct modulation link [10].

Examining this expression indicates that any variation in either the slope efficiency or the responsivity are equally effective at varying the intrinsic gain. For instance, doubling the intrinsic gain value is obtainable by increasing the modulation slope efficiency by $\sqrt{2}$, increasing the photodetection responsivity by $\sqrt{2}$, or increasing both slope efficiency and responsivity by a product equal to $\sqrt{2}$.

Referring to the values of diode laser slope efficiency and photodetector responsivity of the employed modulation and photodetection devices throughout this research, the resultant intrinsic link gain can be computed.

Slope efficiency = 0.3 W/A for the utilized DFB laser diode

Slope responsivity = 0.85 A/W

$$Transmission\ (dB) = 10\log((0.85)^2(0.3)^2) = -11.8692\ dB$$

Clearly, this value is the intrinsic link loss without any amplification stage. But, there is a built-in RF amplifier connected directly at the output of the PIN photodetector of the employed link for this research. The gain of this built-in RF amplifier is frequency dependent; however, this gain is approximately 23 dB. As shown in Section 3.3.1, the optical loss was measured for fiber-optic and FSO links, 3.45 dB and 13.70 dB, respectively. The optical loss has double impact on the overall RF loss. Figure 3.11 illustrates the values of the intrinsic link gain without the built-in RF amplifier, link gain with the built-in RF amplifier, fiber-optic link gain with the RF built-in amplifier, and FSO link gain with the RF built-in amplifier.

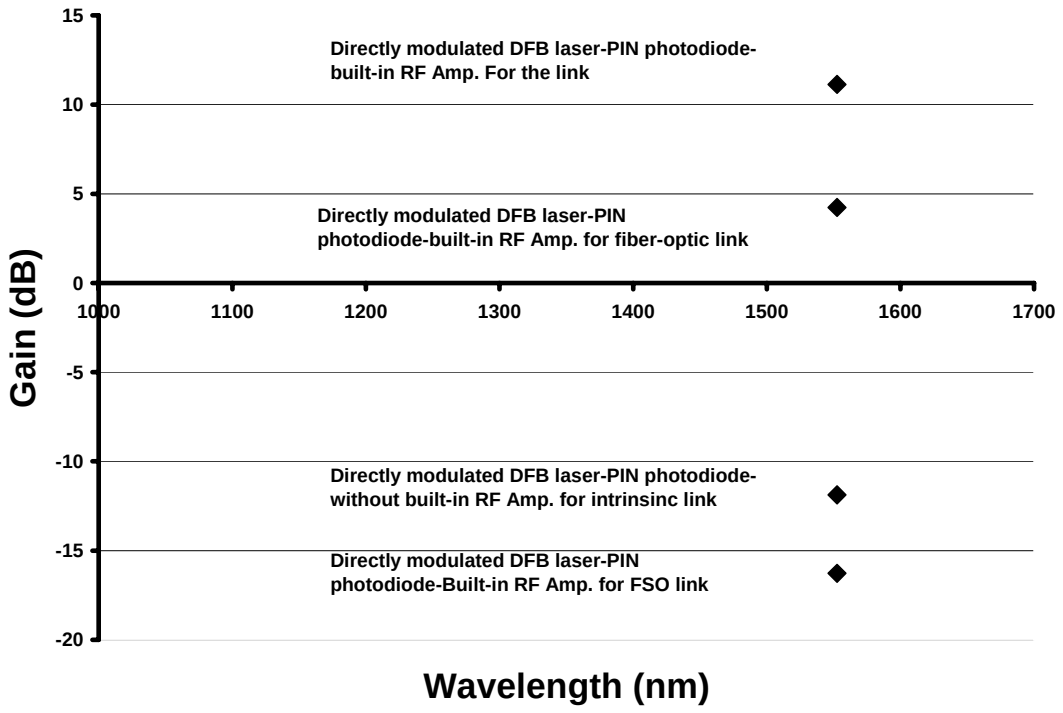

Figure 3.11 plot of gain vs. wavelength for intrinsic link, link with built-in RF amplifier, fiber-optic link with built-in RF amplifier and FSO link with built-in RF amplifier

3.3.3 Reflection Response Measurements and Analysis

Reflection response provides an evaluation of the amount of reflected power relative to the incident power with respect to the signal frequency at the input of the transmitter. The reflected power is predominantly due to impedance mismatch between the RF cable and the input to the analog transmitter, as well as reflections within the transmitter RF/optical conversion circuitry. In determining the RF reflection response, the network analyzer plots the output measurement trace using

$$Reflection(dB) = 10\log\left(\frac{P_{refl}}{P_{inc}}\right) \tag{3.9}$$

where P_{inc} is the RF power measured at the input to the laser transmitter and P_{refl} is the reflected RF power measured at the same input. Results of reflection response measurements for the analog transmitter are the same for both fiber optic and FSO links over the frequency range 55-870 MHz, as shown in Figure 3.12.

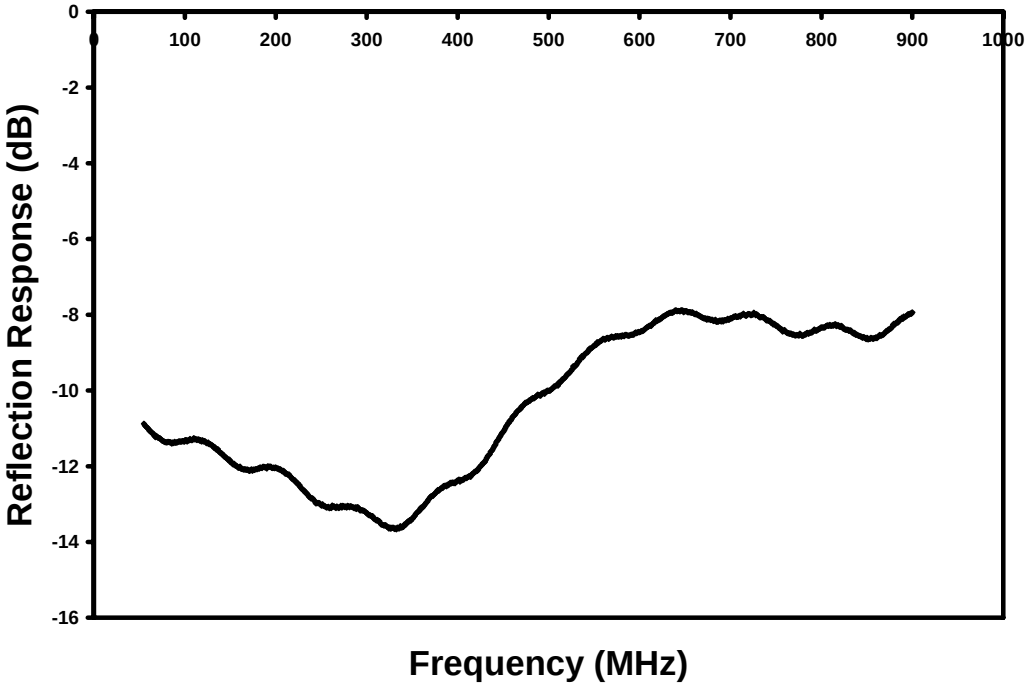

Figure 3.12 Reflection response measurements.

3.3.4 Group Delay Measurements and Analysis

The group delay is a measure of the total time a signal experiences when traversing a communications link, which thus creates a phase shift in the signal. Ensuring that the group delay does not vary considerably with frequency indicates that a communications channel does not introduce phase distortion. The group delay measurements for the fiber-optic link, with and without the RF amplifier included, are illustrated in Figure 3.13. Note that, without the RF amplifier, the group delay has an approximately constant average value of 84.70 ns. The RF amplifier introduces quite

a bit of variation in the group delay below 125 MHz, but settles to an approximately constant average value of 93.62 ns above 125 MHz. Thus, without the RF amplifier, phase distortion is so small over the 55-870 MHz operating range of the fiber-optic link as to be negligible. With the RF amplifier, operation should be bounded to an operating range of 125-870 MHz if phase distortion is to be reduced [26].

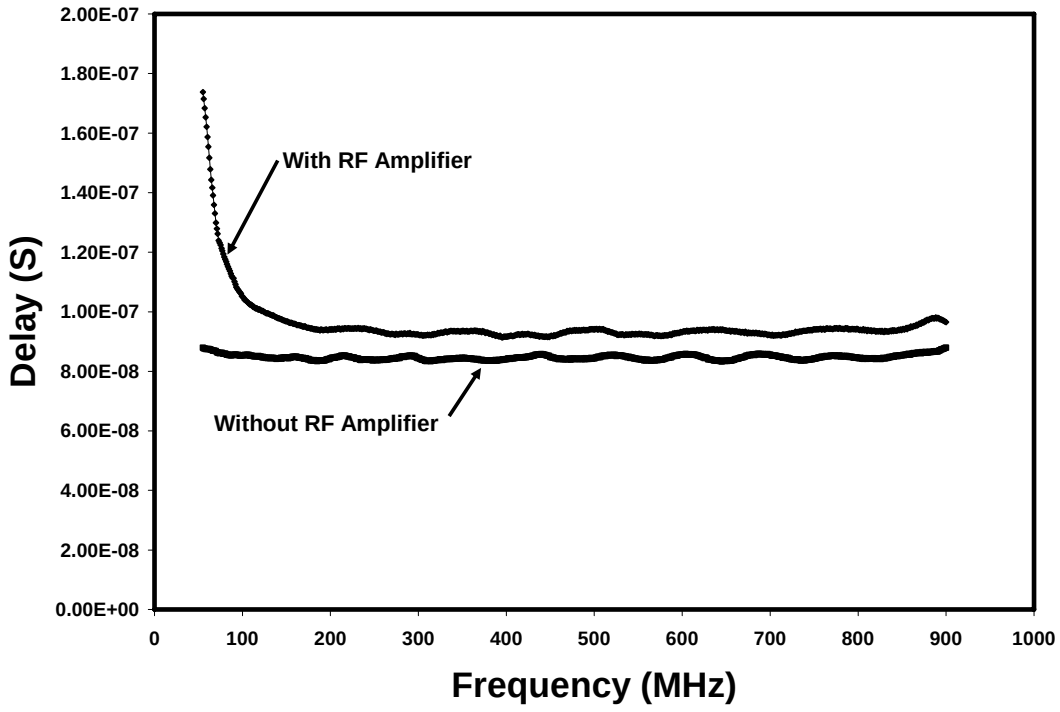

Figure 3.13 Group delay measurements for fiber-optic link.

Results of group delay measurements for the FSO link are shown in Figure 3.14. Clearly, without the RF amplifier, the group delay has a nearly constant average value

of 79.66 ns. With the RF amplifier, the group delay has quite a bit of variation below 110 MHz, but settles to an approximately constant average value of 90.22 ns above 110 MHz. Similarly, without the RF amplifier, little phase distortion can be seen over the 55-870 MHz operating range of the FSO link. With the RF amplifier, operation should be limited to an operating range of 110-870 MHz if phase distortion is to be avoided. Obviously, the speed of light in free-space is faster than that in the fiber, as shown in the measured values of the group delays in both links [26].

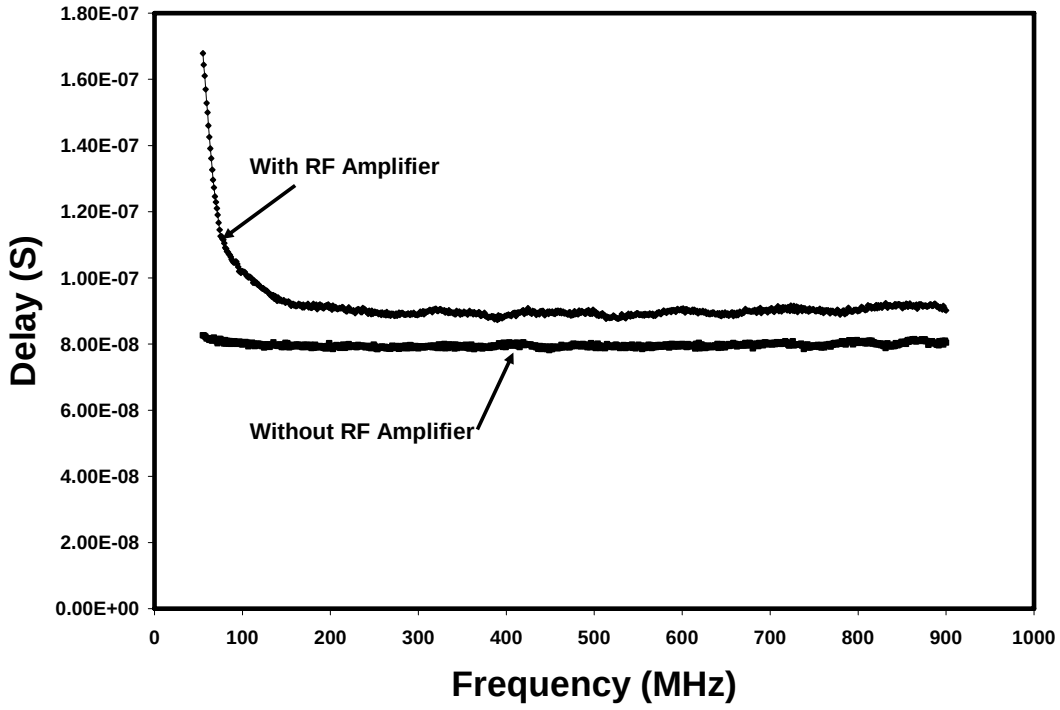

Figure 3.14 Group delay measurements for free-space optic link.

3.3.5 CNR Measurements and Analysis

Carrier-to-noise ratio (CNR) is an important measure which quantifies the performance of communication channels relatively to the existing noise. CNR plays an important role in determining the minimum average signal power that can provide error-free transmission through a communications channel.

For this investigation, CNR measurements were performed for both fiber optic and FSO links, with and without the RF amplifier, over a frequency range of 55-870 MHz. The RF output power from the signal generator was 0 dBm for all measurements. The results of the CNR measurements for fiber-optic link are shown in Figure 3.15. Without the RF amplifier, the CNR varied between 40.75 dB and 58.13 over the frequency range 55-850 MHz, while CNR with the RF amplifier varied between 58.54 dB and 73.15 over the same frequency range. These values compare favorably with results from CNR measurements on other analog fiber optic links reported in [4, 11].

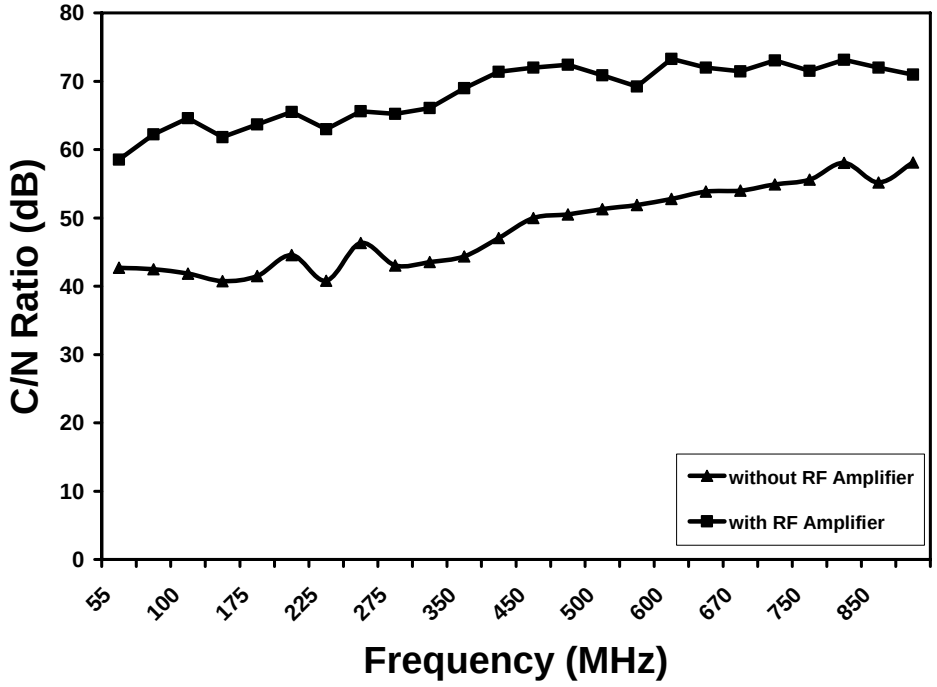

Figure 3.15 CNR measurements for fiber-optic link.

The results of CNR measurements for the FSO link are shown in Figure 3.16. Without the RF amplifier, the CNR starts at minimum value of 17.52 dB at 55 MHz and trends upward with increasing frequency to a maximum value of 46.55 dB at 850 MHz. With the RF amplifier, the CNR starts out at a minimum value of 43.52 at 55 MHz and trends upward with increasing frequency to a maximum value at 63.3 dB at 850 MHz. These values compare favorably with results of CNR measurements of the previous fiber-optic link. Therefore, FSO can be a viable replacement for fiber optics in short distance implementations.

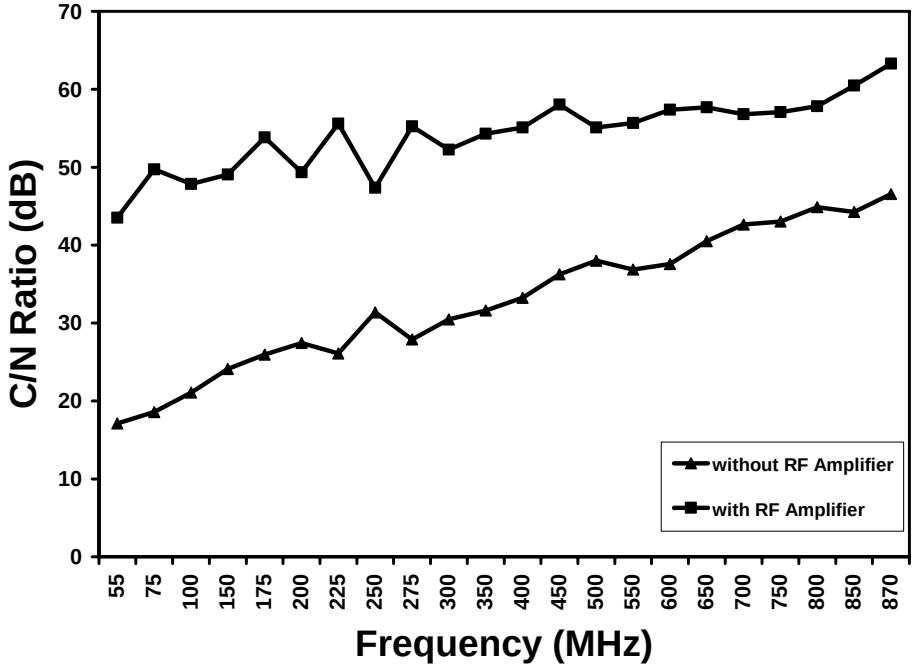

Figure 3.16 CNR measurements for free-space optic link.

3.3.6 Link Noise Figure

The noise figure for directly modulated link is dominated by the laser source RIN. Figure 3.17 illustrates the thermal noise sources at the laser transmitting side of the directly modulated link and the laser source RIN at the receiving side of the link.

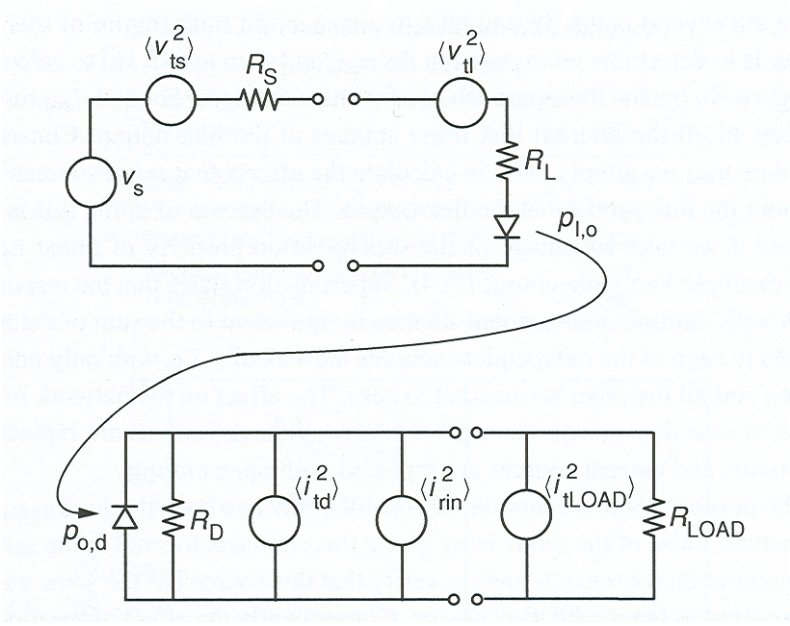

Figure 3.17 Directly modulated link[10]

Assuming the presence of the impedance matches at both ends of the link with the RF input and output, and also assuming that the load resistance is equal to the source resistance.

It is important to define n_{extra}, so that the noise figure of this circuit can be determined using Eq. (2.9). Clearly, Eq. (2.10) shows that n_{extra} represents the impacts of all internal link noise sources at the link output. Computing n_{extra} is carried out by calculating all the impacts that noise sources located throughout the link produce at the link output. Taking the advantage of the superposition property of linear networks simplifies these calculations. For the purpose of this employed link used throughout this dissertation, only two contributions to n_{extra} have been considered:

1. Thermal noise of the laser diode which has output power equal to $g_{rf}\,kT$

2. RIN source which has noise power equal to $\left\langle i_{RIN}^2 \right\rangle R_{Load}$

Practically, there are additional noise sources at the photodiode side of the link, two of them are shown in Figure 3.17; the thermal noises from the photodiode resistance and the load resistance. Typically, the RIN and/or the photodiode current are sufficiently high that the RIN dominates over the thermal noise sources in the majority of the analog link designs.

The remaining noise power that need to be evaluated is n_{in}, which is just the thermal noise power of the source resistor; hence $n_{in} = kT$.

Substituting these three terms into Eq. (2.11) produces an expression for the noise figure of a RIN-dominated, directly modulated link with passive magnitude impedance matching, which is the link used through this investigation:

$$NF = 10\log\left(1 + \frac{g_{rf}kT + \left\langle i_{RIN}^2 \right\rangle R_{Load}}{g_{rf}kT}\right) = 10\log\left(2 + \frac{\left\langle i_{RIN}^2 \right\rangle R_{Load}}{s_t^2 \eta_r^2 kT}\right) \qquad (3.10)$$

Substituting the employed component parameters, which are shown in table 3.1, plots the noise figure versus RIN noise source can be obtained.

Table 3.1 Analog link parameter values

Parameter	Value
Laser slope efficiency (W/A)	0.3
Photodiode responsivity (A/W)	0.85
Photodiode load resistance (Ohm)	75
Average photodiode current (mA)	1
Temperature (K)	290

Figure 3.18 shows that when the RIN increases, the noise figure also increases. When the RIN approaches zero, the noise figure doesn't approach zero, which indicates that the minimum noise figure can be at least 3 dB.

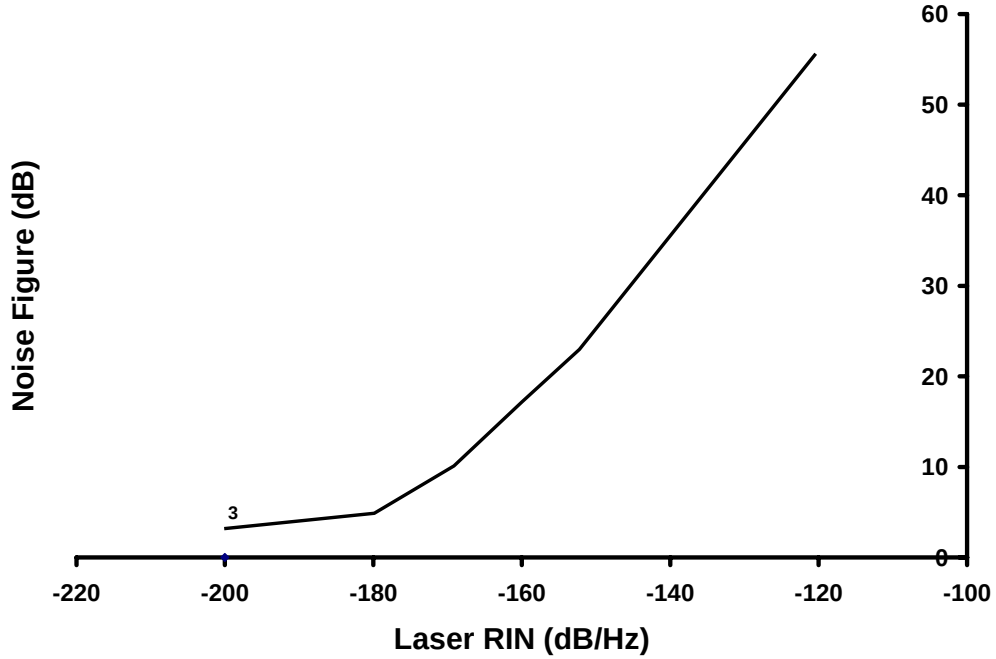

Figure 3.18 Noise figure vs. laser RIN

3.3.7 Dynamic Range Measurements and Analysis

There are two principal methods used to measure the dynamic range as mentioned in chapter 2 [10]:

I. Insert a single RF sinusoid signal ω through the optical link and measure the resulting second and third order harmonic distortions at 2ω *and* 3ω respectively.

II. Insert two sinusoidal RF signals of equal amplitude and close in frequency spacing through the optical link and measure the second order intermodulation distortion at $\omega_2 + \omega_1$ or $\omega_2 - \omega_1$ and the third order intermodulation distortion at $2\omega_1 - \omega_2, 2\omega_2 - \omega_1, 2\omega_1 + \omega_2, 2\omega_2 + \omega_1$. Narrowband links allow the frequencies $2\omega_1 - \omega_2$ and $2\omega_2 - \omega_1$ to pass and eliminate the rest.

The second method is the more convenient way of measuring the dynamic range and was used in this dissertation. The third order intermodulation (3IM) power was measured to introduce the 3IM free dynamic range. An RF multiplexer was used to mix two equal power RF signals at closely spaced frequencies of $f_1 = 499\,MHz, f_2 = 501\,MHz$. Inserting the result RF signal into the FSO channel, the 3IM signal power was measured at frequencies

$2f_1 - f_2 = 497\ MHz,\quad and\quad 2f_2 - f_1 = 503\ MHz.$ Going over the same measurements while increasing the input power for both frequencies allows the 3IM line to be drawn. Measuring the output power of the fundamental frequency $f = 500\ MHz$ over the same range of input power allows the fundamental output line to be drawn, which intersects the 3IM line. In this study, a directly modulated, distributed feedback (DFB) laser diode was used as the transmitter, so RIN is the dominant noise source.

Table 3.2 shows the component parameters for the fiber-optic link under test. The 3IM free dynamic range was found to be 101 dB.Hz$^{2/3}$, as shown in Figure 3.19. Previous studies have reported a typical 3IM free dynamic range of 116 dB.Hz$^{2/3}$ for the CATV application over fiber-optic links [10, 11, 36, 37]. Therefore, the measured result is acceptable compared to the reported result. The decrease in the measured 3IM free dynamic range results from the built-in RF amplifier (a nonlinear device) at the output of the photodiode.

Table 3.2 Fiber-optic link parameters

Optical wavelength	λ	1552.524 nm
Optical output power	P_o	10 dBm
Laser Noise	RIN	-159 dBm
Optical Modulation Index	MOI	8.8%/channel
Modulator Impedance	R_m	75 Ohm
Optical link Loss	L_o	3.45 dB
Photodiode Responsivity	η_p	0.85 A/W
Photodiode Load	R_p	75 Ohm
Noise Bandwidth	BW	1 Hz

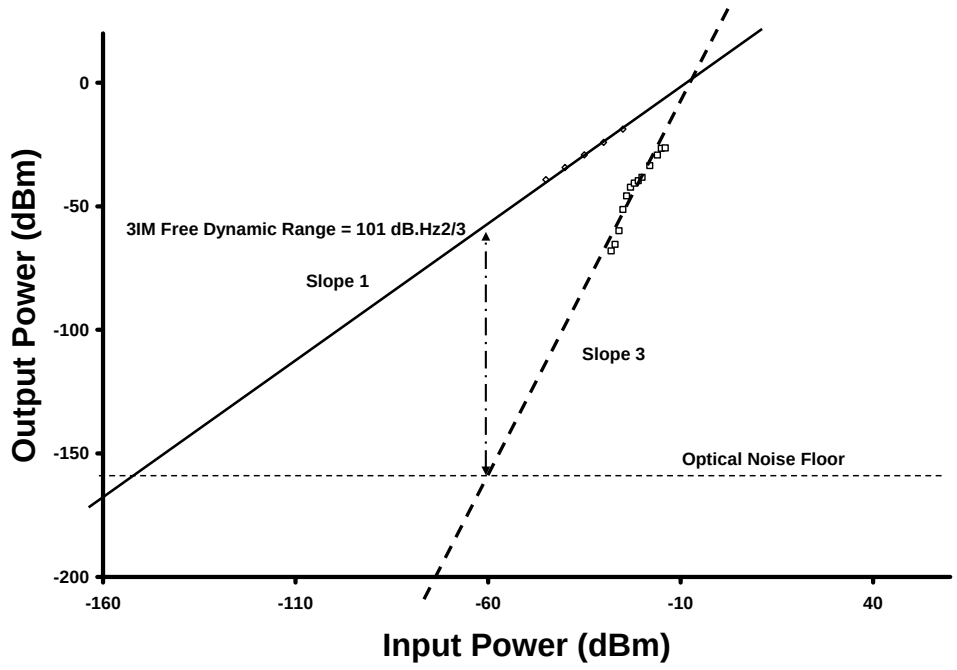

Figure 3.19 Third order intermodulation free dynamic range measurements for fiber-optic link.

Table 3.3 shows the component parameters of the FSO link under test. The 3IM free dynamic range was found to be 101 dB.Hz$^{2/3}$, as shown in Figure 3.20. This value compares favorably with the previously mentioned measured value for the fiber-optic link under test and indicates the absence of any nonlinear devices. From a distortion viewpoint, both fiber-optic and FSO links act similarly. However, the addition of an optical amplifier to the FSO link to increase span length would lead to increased distortion.

Table 3.3 Free-space optical link parameters

Distributed Feedback (DFB)	λ	1552.524 nm
Optical output power	P_o	10 dBm
Laser Noise	RIN	-159 dBm
Optical Modulation Index	MOI	8.8%/channel
Modulator Impedance	R_m	75 Ohm
Optical link Loss	L_o	13.70 dB
Photodiode Responsivity	η_p	0.85 A/W
Photodiode Load	R_p	75 Ohm
Noise Bandwidth	BW	1 Hz

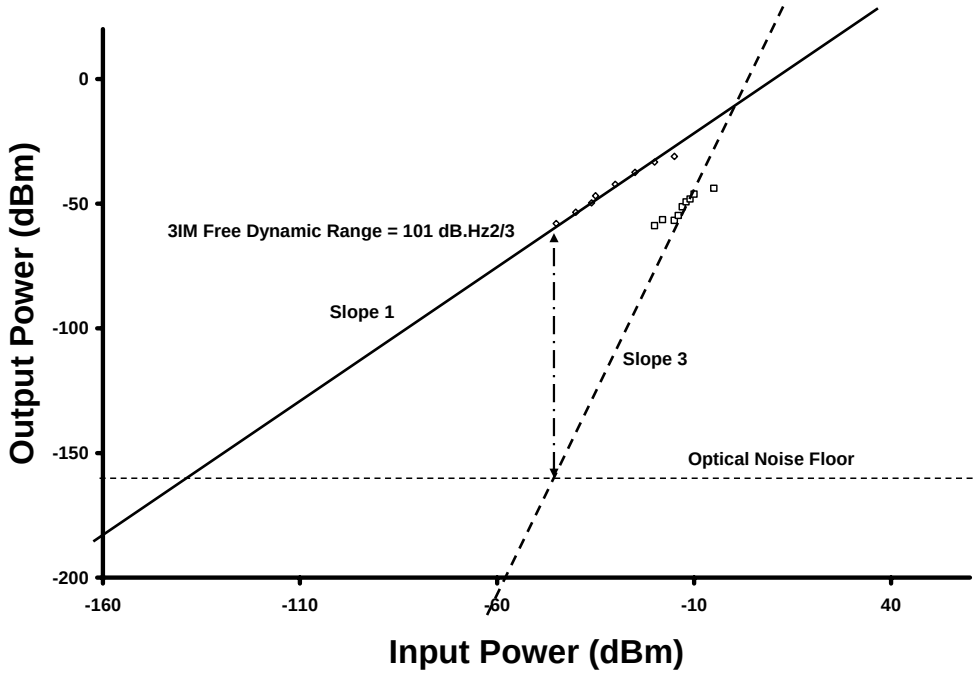

Figure 3.20 Third order intermodulation free dynamic range measurements for free-space optic link.

3.8 Summary

This chapter presents a comparison of key performance measures for a FSO link versus a fiber optic link for the transport of analog RF signals. The comparative study consists of experimental data, supported with theoretical analysis, collected from optical power, transmission response, reflection response, group delay, CNR, and dynamic range measurements. The data shows that FSO is suitable for RF transmissions and performs comparably with similar fiber optic links. When direct line-of-sight is available between two locations, FSO can offer an attractive alternate for fiber optic links to transport modulated RF analog signals over short distances.

Chapter 4

The Transmission of Cellular Signals over Free-Space Optical Links to Base Stations from Macro-and Microcells

4.1 Introduction

With the increasing demands of transporting voice, data, and video traffic over cellular networks, the IS-95 standard known as Code Division Multiple Access (CDMA) is replacing Time Division Multiple Access (TDMA) technologies to provide an effective and efficient means of meeting these demands. IS-95 CDMA is capable of setting up communication channels between various mobile users and their base stations with different bandwidth requirements depending on the quantity of data to be transferred. CDMA cells employ a direct sequence spread spectrum (DSSS) technique and share a common frequency band for communication. Users are distinguished from each other by each using a different pseudo-code sequence for spectrum spreading.

In a typical urban area, cellular network providers deal with increasing traffic demands by installing more cells while simultaneously shrinking their geographic coverage to support a larger number of subscribers. Macrocells exhibit coverage over

several kilometers and their antennas are mounted on the rooftops of tall buildings or on towers. For regions with high population densities, microcells are used to provide coverage with their antennas installed on buildings below rooftop height. The macrocell and microcell antennas are linked to their respective base stations which convert the air-interface (wireless) protocols to wireline infrastructure protocols. Researchers have recently investigated the possibility of transporting modulated Radio Frequency (RF) signals, including those in the form of CDMA signals, over analog fiber optic links [38]. These investigations have produced promising results, but the installation expense for optical fiber infrastructure is high in metropolitan areas. This chapter proposes and examines an attractive method of transporting IS-95 CDMA channels to their respective base stations using FSO links, as shown in Figure 4.1.

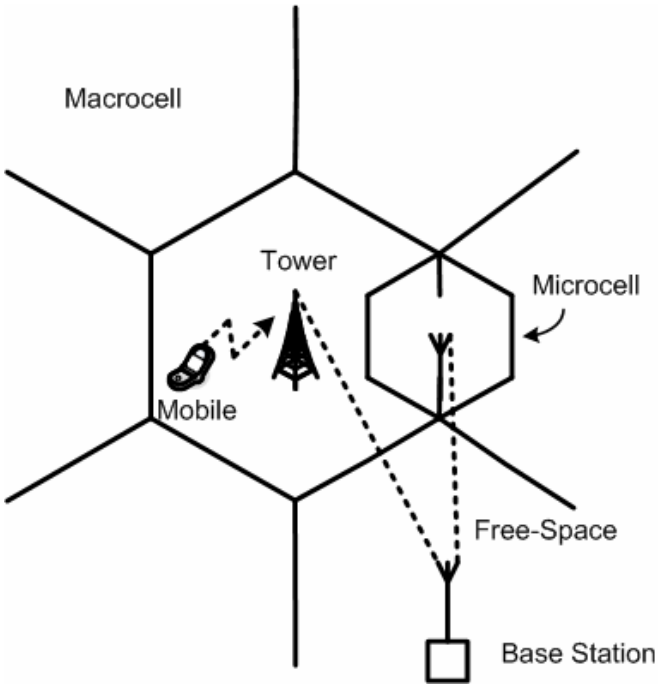

Figure 4.1 Diagram of a base station connected to both a macrocell and microcell using a FSO link.

While the transmission of IS-95 CDMA forward and reverse channels as RF intensity-modulated signals over fiber optic links has been explored elsewhere[39], this chapter specifically investigates the use of FSO technology to transport modulated IS-95 CDMA analog signals.

The *advantages* of FSO links for transmission of modulated IS-95 CDMA forward and reverse channels are as follows:

1. FSO IS-95 CDMA links can be installed *faster* and at considerably *less expense* than fiber optic links for distances up to 4 km.

2. FSO links provide enhanced link *security*, much higher *immunity* from Electromagnetic Interference (EMI), and do not need *licensing* when compared with wireless RF links, or directional microwave links.

3. The incorporation of FSO provides methods to lower the expense to setup temporary IS-95 CDMA microcells by eliminating the need for demodulating and dispreading equipment. Temporary microcells are frequently deployed for special events, e.g. a football game, where a large number of cellular subscribers are temporarily gathered together. Thus the equipment required at such a cell site consists of simply an antenna, RF amplifiers, analog transmitter, analog receiver, optical amplifier, and FSO collimating telescopes, as shown in Figure 4.2.

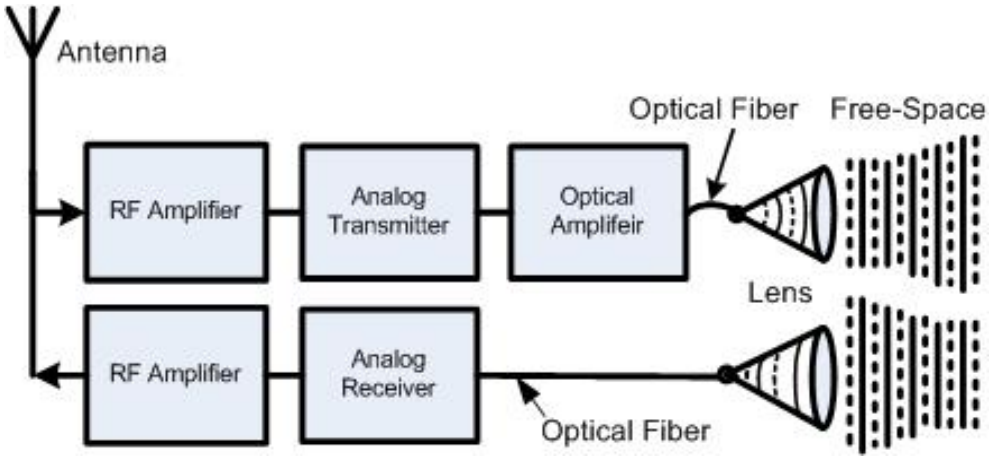

Figure 4.2 Typical equipment found at a microcell that uses an analog FSO link to communicate with a base station.

The *objective* of this chapter is to characterize the forward and reverse channels established when a modulated analog IS-95 CDMA signal is transported over an FSO link. In the following subsections, the experimental setup is described and the experimental results and analysis are reported.

4.2 Experimental Setup

Figure 4.3 shows the experimental setup utilized in IS-95 CDMA user power and SNR measurements. An Aurora AT3510 analog laser transmitter, with an ITU grid compliant output wavelength of 1554.134 nm, was coupled to a Dominion Lasercom DAViD® FSO telescope assembly by a single-mode optical fiber. The transmitting and receiving telescopes were aligned line of sight toward each other and separated by a distance of 3 m. The receiving telescope, also a Dominion Lasercom DAViD® FSO telescope assembly, was coupled to an Aurora AR4001 analog receiver by a single-mode optical fiber. The IS-95 CDMA input signal applied to the transmitter was produced by an Rohde & Schwarz SMIQ 06B signal generator capable of generating CDMA uplink channels (mobile to base station) and CDMA downlink channels (base station to mobile) using frequencies from 869 to 894 and from 824 to 849 MHz, respectively. The RF output signal from the receiver was linked to a Tektronix WCA280A wireless communication analyzer to capture SNR measurements or connected to an Agilent E7485A base station test receiver to capture IS-95 user channel measurements. The Agilent CDMA test receiver demodulates and

dispreads the RF output signal to obtain user power measurements. All measurements were conducted without the external RF amplifier. While an RF amplifier can be coupled at the receiver output to provide RF signal gain, it is beyond the focus of this study.

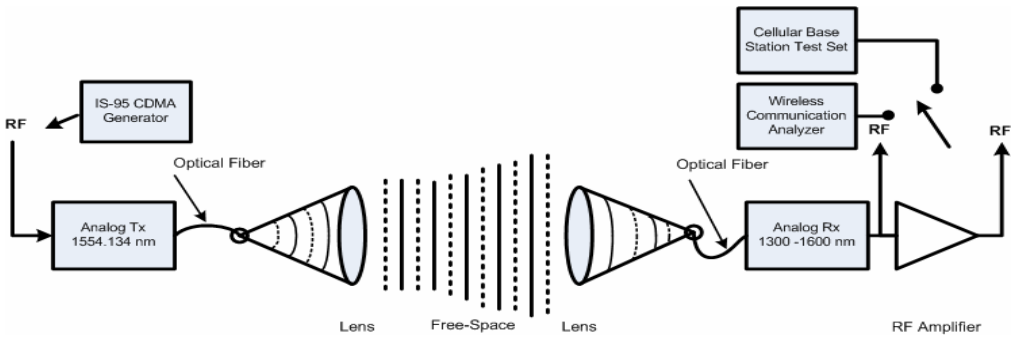

Figure 4.3 The experimental setup for measuring user power and SNR when IS-95 CDMA is transported over a FSO link.

4.3 Experimental Results and Analysis

In this section, the results achieved using the experimental setup described in Sec.4.2 are reported. The results include measurements of user power and SNR. These measurements provide the required data to describe the characteristics of the overall IS-95 CDMA forward and reverse communication channels, including the double conversions and the free-space signal propagation.

4.3.1 IS-95 CDMA User Power Measurements and Analysis

The forward IS-95 CDMA channel (base station to mobile) is characterized in terms of frequency and a code sequence. Sixty-four *Walsh Codes* are used to describe the down link channels, providing 64-physical channels. The IS-95 forward channel contains four different types of channels -- W_0 pilot channel, W_{32} synchronization channel, W_1 paging channel, and (W_2-W_{31}) and (W_{33}-W_{63}) traffic channels. A base station distinguishes among its CDMA mobile users by appointing a different Walsh code for each mobile user in its service coverage.

In the beginning, CDMA power measurements were completed directly at the output of the CDMA signal generator, without including FSO equipment. These measurements present base line values that would be used for comparison. Figure 4.4 shows power measurements achieved from the Agilent E7495A base station test receiver. It represents the 64 physical channels and power measurements for the IS-95 CDMA forward channel. The W_0 pilot power, W_{32} delta synchronization power, W_1 delta paging power, and channel power were measured and found to be -6.9 dBm, -15 dB, -11.8 dB, and 0 dBm, respectively. The pilot power is approximately 4-6 dB stronger than all other channels. The delta synchronization power is the amplitude difference between the sync power and pilot power, the delta paging power is the amplitude difference between the paging power and pilot power, and the channel power is the power transmitted across the entire 1.25 MHz CDMA channel set at 0 dBm. Power measurements were captured after the installation of free-space channel setup.

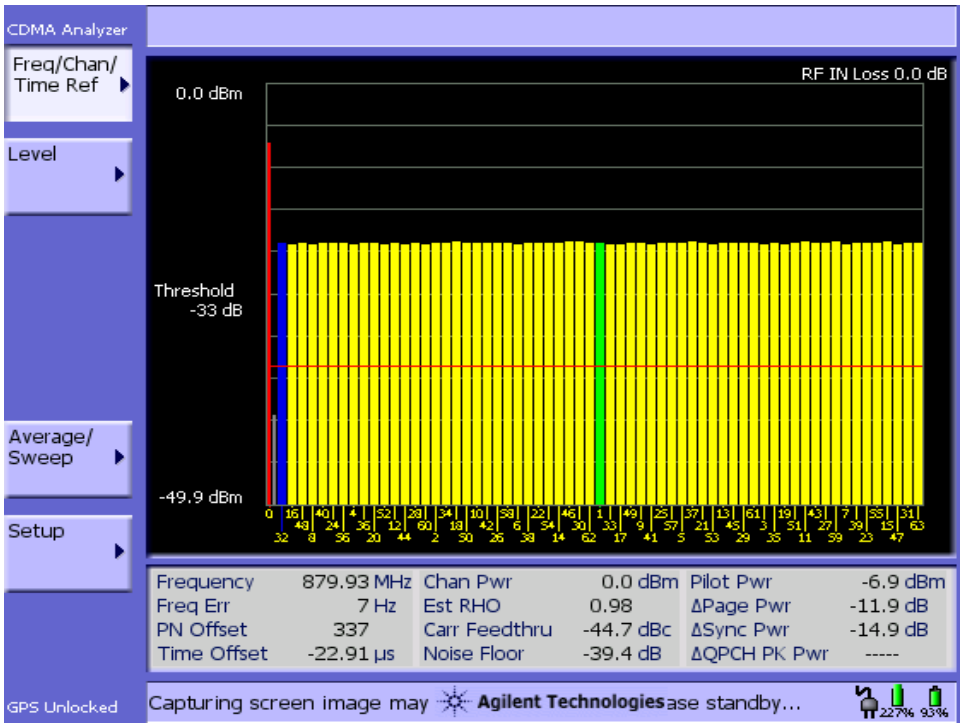

Figure 4.4 A screen capture from the Agilent E7495 A base station test set illustrating the results of forward channel measurements at the output of the IS-95 CDMA generator.

Figure 4.5 illustrates the results of the IS-95 CDMA forward channel measurements at the output of the analog receiver. The W_0 pilot power, W_{32} delta synchronization power, W_1 delta paging power, and channel power were measured and found to be -21.9 dBm, -14.5 dB, -11.7 dB, and -14.6 dBm, respectively.

The pilot channel is the beacon for its related base station. Each mobile user constantly monitors the detectable pilot signals from adjacent base stations to handoff to the strongest base station when the handoff is considered necessary. T_ADD is the *pilot detection threshold* that defines the adequate pilot strength that could keep the

mobile user connected to its base station. When compared to the value of the pilot power at the receiving side with the range of values of T_ADD (-31.5 - 0 dB) reported in [39], the pilot power measured here is within the reported limits.

The reverse IS-95 CDMA channel (mobile to base station) is also characterized in terms of a frequency and a code sequence. The RF carriers extend across the range 869-894 MHz, whereas the code sequence is a unique, long pseudo random PN code offset used to define the uplink channels. The W_0 pilot power and channel power were measured and found to be -15.8 dBm and -14.6 dBm, respectively. The value of the reverse channel power is determined by the base station through which the mobile terminal is communicating. To sustain a uniform power received from mobile terminals, regardless of their positions with respect to the base station, the base station implements a complex power control algorithm to guide mobile terminals to lower or higher their transmission power (reverse channel power).

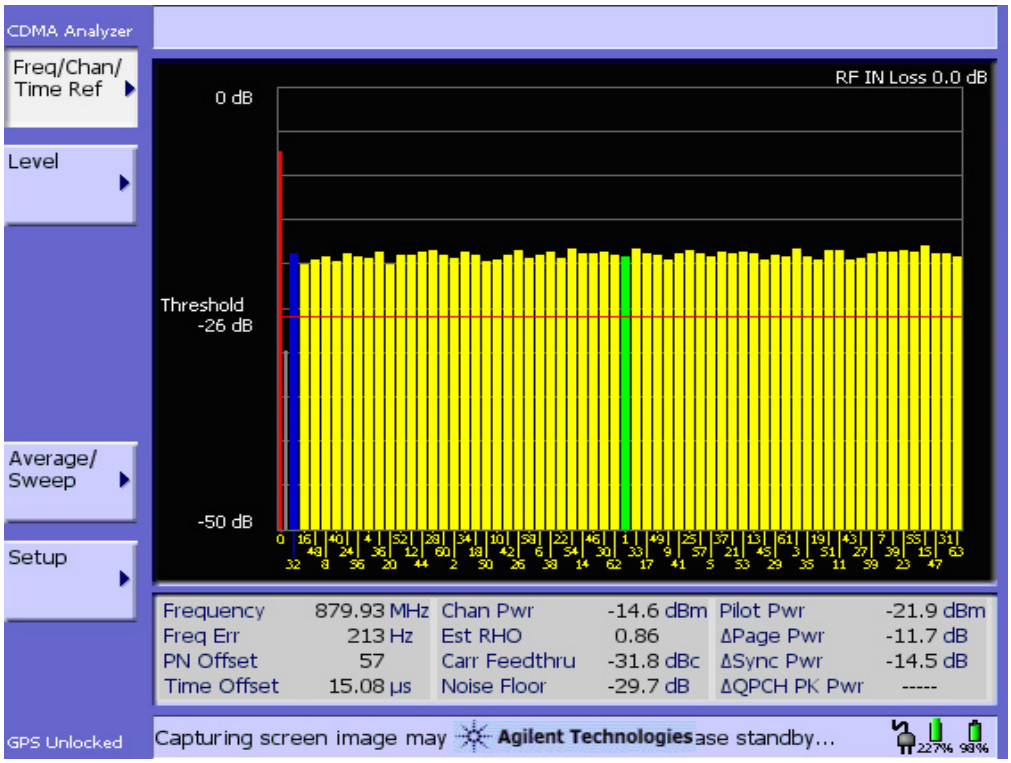

Figure 4.5 A screen capture from the Agilent E7495 A base station test set illustrating the results of IS-95 CDMA forward channel measurements at the output of the analog receiver.

The objective of the algorithm is to reduce interference among mobile terminals and thus increase base station capacity. During the measurements, the IS-95 CDMA reverse channel power was set at 0 dBm. This power can be increased to 23 dBm, depending on the neighboring environments.

4.3.2 SNR Measurements and Analysis

The RF carrier of the IS-95 CDMA channel occupies 1.25 MHz of the band as measured and shown in Figure 4.6. The transmission of this carrier through a FSO link, instead of a conventional RF or a microwave link, exposes the signal to different types of noise. As mentioned in Chapter 2, the sources of noise in a FSO link consists of relative intensity noise (RIN) generated by the laser transmitter, shot noise generated by the photodiode in the receiver, and thermal noise generated by resisters throughout the link circuitry. SNR measurements versus frequency were carried out for IS-95 CDMA forward and reverse channels over FSO.

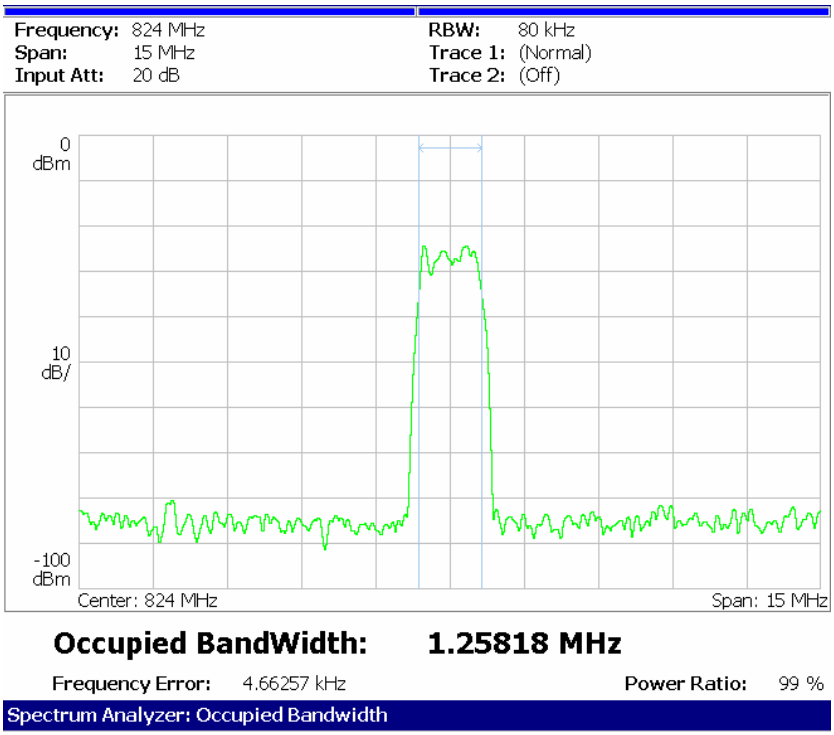

Figure 4.6 Occupied bandwidth of IS-95 CDMA signal

The RF output power of the IS-95 CDMA generator was placed to 0 dBm for all SNR measurements. The results of the forward link SNR measurements at the receiving side are shown in Figure 4.7. The SNR has a minimum value of 40.5 dB at 824 MHz and trends upward with increasing the frequency to a maximum value of 46.5 dB at 849 MHz. The required SNR for an IS-95 CDMA forward link is at least 16 dB, depending on the mobile users' environments [39], so the results measured are considerably better.

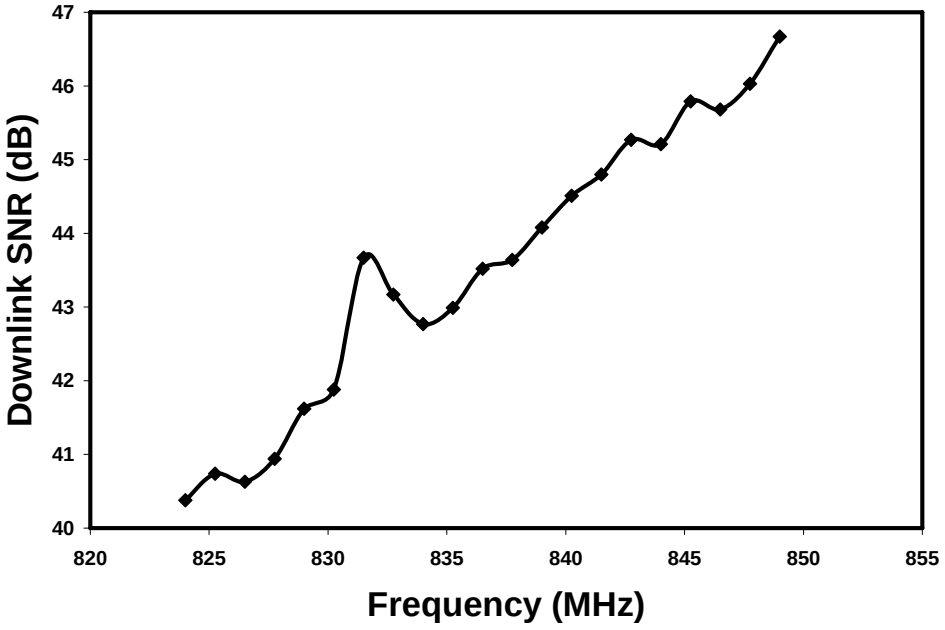

Figure 4.7 Results of SNR measurements for the forward channel.

The results of the reverse link SNR measurements at the receiving side are shown in Figure 4.8. The largest power that a mobile user can transmit is 23 dBm, depending on the power control loop. The RF output power of the IS-95 CDMA generator was

set at 0 dBm for all measurements. SNR measurements varied around an average value of approximately 40.75 dB throughout the IS-95 CDMA reverse range of frequencies (869-894 MHz). The typical SNR for IS-95 CDMA reverse links may vary by over 7 dB, depending on the power control and soft handoff algorithms [39]. The results measured here are considerably better than the required values.

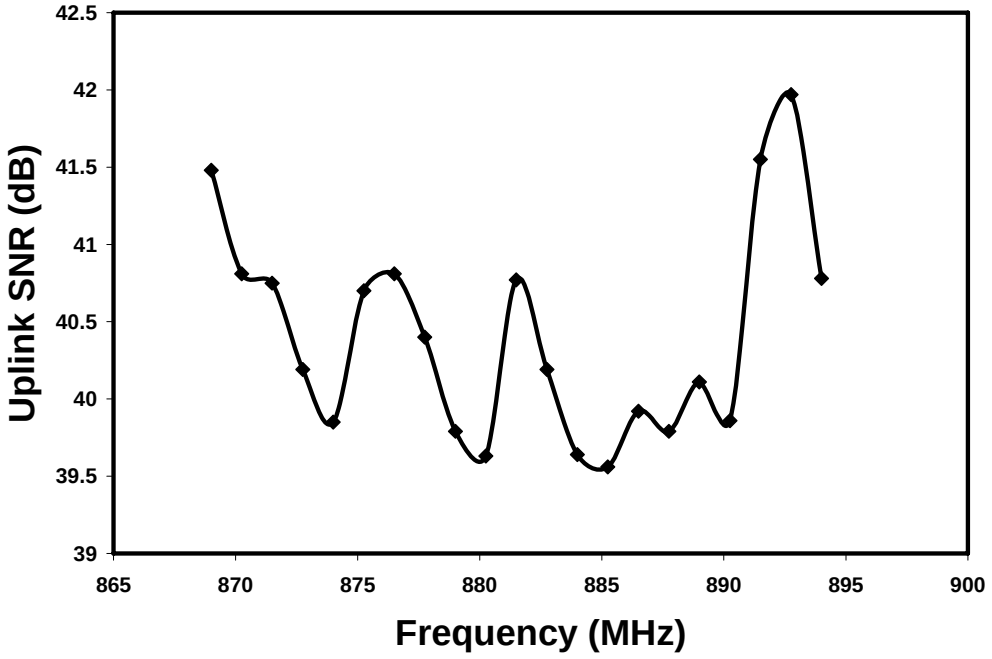

Figure 4.8 Results of SNR measurements for the reverse channel.

4.4 Summary

This chapter has described an investigation into the viability of FSO for transporting IS-95 CDMA signals to base stations. Experimental measurements of user power and SNR demonstrate that FSO offers a suitable transport medium when compared with other published data, with performance that exceeds other transmission techniques.

Further, FSO has several features that should lead to a significant role for its application to IS-95 CDMA transmission in the future.

Chapter 5

The Deployment of *CATV* Signals over Free-Space Optical Links

5.1 Introduction

Cable television or community antenna television (CATV) is a technology that employs radio frequency (RF) signals to broadcast video traffic over a variety of transmission media. Growing consumer demands for new high-speed services and expense containment factors have led CATV service providers to deploy increasing amounts of optical fiber as the transmission medium of choice. Additional, using dense wavelength division multiplexing (DWDM) technology, CATV providers are able to transmit tens of CATV channels over single optical fiber. However, the cost of installing new fiber infrastructure in metropolitan environments can be quite high. In this chapter, an attractive method of transporting CATV using point-to-point FSO links is proposed and examined. In particular, this chapter investigated the transmission of two wavelength division-multiplexed VHF and UHF channels over a FSO link for potential CATV applications.

In the following subsections, the experimental setup is described and the experimental results and analysis are reported.

5.2 Experimental Setup

Figure 5.1 shows the experimental setup used for RF transmission response measurements. Two Aurora AT3510 analog laser transmitters, with ITU grid compliant output wavelengths of 1552.524 nm and 1554.134 nm, were wavelength division-multiplexed using an Aurora OP35M4C multiplexer. The resulting signal was fiber-coupled to a Dominion Lasercom DAViD® FSO telescope assembly, shown in Figure 5.2. The space gap separating the aligned transmitting and receiving telescopes was 3 m, which was adequate to characterize the proof-of-concept, end-to-end communication channel, less the atmospheric and geometric losses. The atmospheric loss suffered by FSO systems has been widely studied, as explained in Chapter 2. The receiving telescope, also a Dominion Lasercom DAViD® FSO telescope assembly, was fiber-coupled to an Aurora OP31D2D demultiplexer to extract the transmitted wavelengths from the obtained composite signal. Two Aurora AR4001 analog receivers were linked to the outputs of the demultiplexer. The RF operating frequency range for the transmitters and receivers was from 46 MHz to 870 MHz.

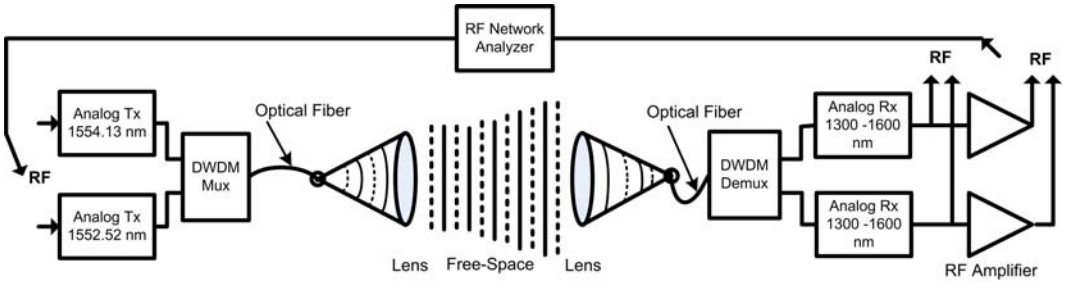

Figure 5.1 FSO experimental setup for RF transmission response measurements.

For transmission response measurements, an Agilent 8712ET RF vector network analyzer was coupled between the transmitter input and receiver output. In addition, Aurora OA4444T-42 RF amplifiers were coupled between the receiver outputs and the input of the network analyzer, as a result providing RF signal gain. The Aurora equipment used in this investigation was manufactured mainly for the CATV industry.

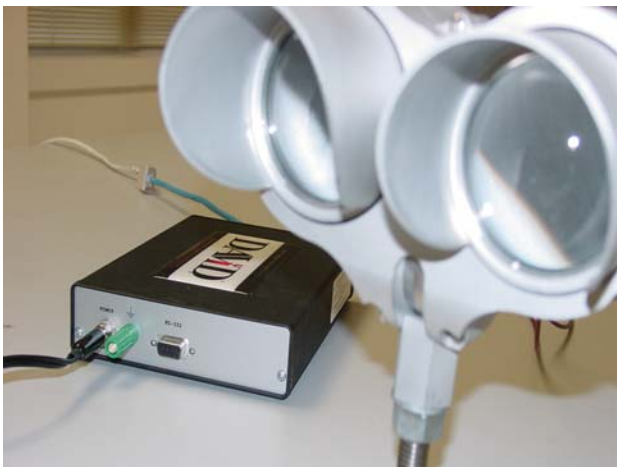

Figure 5.2 Dominion Lasercom DAViD® FSO System.

For the dynamic range measurements, the only main modification in the setup from Figure 5.1 was that, upon removal of the vector network analyzer, Rohde & Schwarz SMHU and Agilent 8642A signal generators were coupled to the transmitter inputs to provide the composite RF input signals. A Tektronix WCA280A wireless communication analyzer was used as an RF spectrum analyzer to measure the output signals, as shown in Figure 5.3.

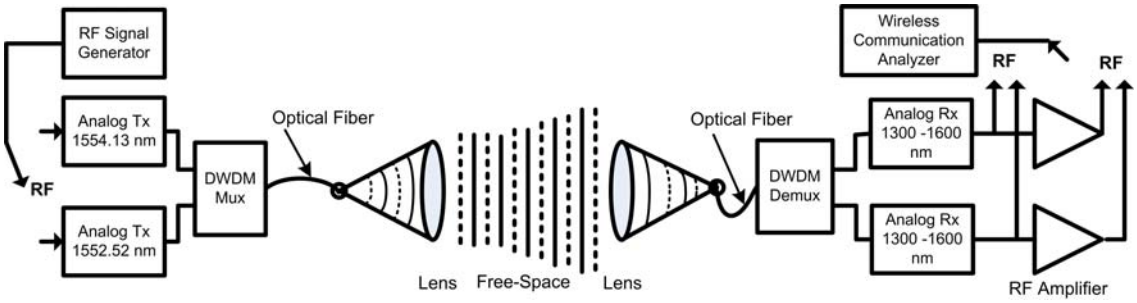

Figure 5.3. FSO experimental setup for dynamic range measurements

5.3 Experimental Results and Analysis

5.3.1 Optical Power Measurements and Analysis

This section presents results from optical power measurements conducted on the FSO link and addresses the main sources of optical loss. The peak optical powers and output wavelengths of the analog laser transmitters, after being wavelength division

multiplexed, were measured using an Advantest Q8384 optical spectrum analyzer. Peak powers of 7.56 dBm and 7.22 dBm, and their respective output wavelengths of 1552.53 nm and 1554.13 nm, were measured at the output of the multiplexer on the transmitting end. These values are shown in the lower table of Figure 5.4. These measurements were taken again at the input of the demultiplexer on the receiving end. Peak powers of -12.24 dBm and -12.47 dBm, and respective output wavelengths of 1552.53 nm and 1554.13 nm, were measured. These values are shown in the lower table of Figure 5.5. Clearly, there is a loss in optical power of nearly 19 dB. Compared with other previously reported results for single wavelength transmission over FSO links, this loss is nearly 4 dB higher. After careful examination, the source of this additional loss is not apparent and is left as a topic for future investigation. Also, transporting multiple RF signals over single fiber-optic link demonstrated more optical loss when compared to that for single RF signal over single fiber-optic link [11].

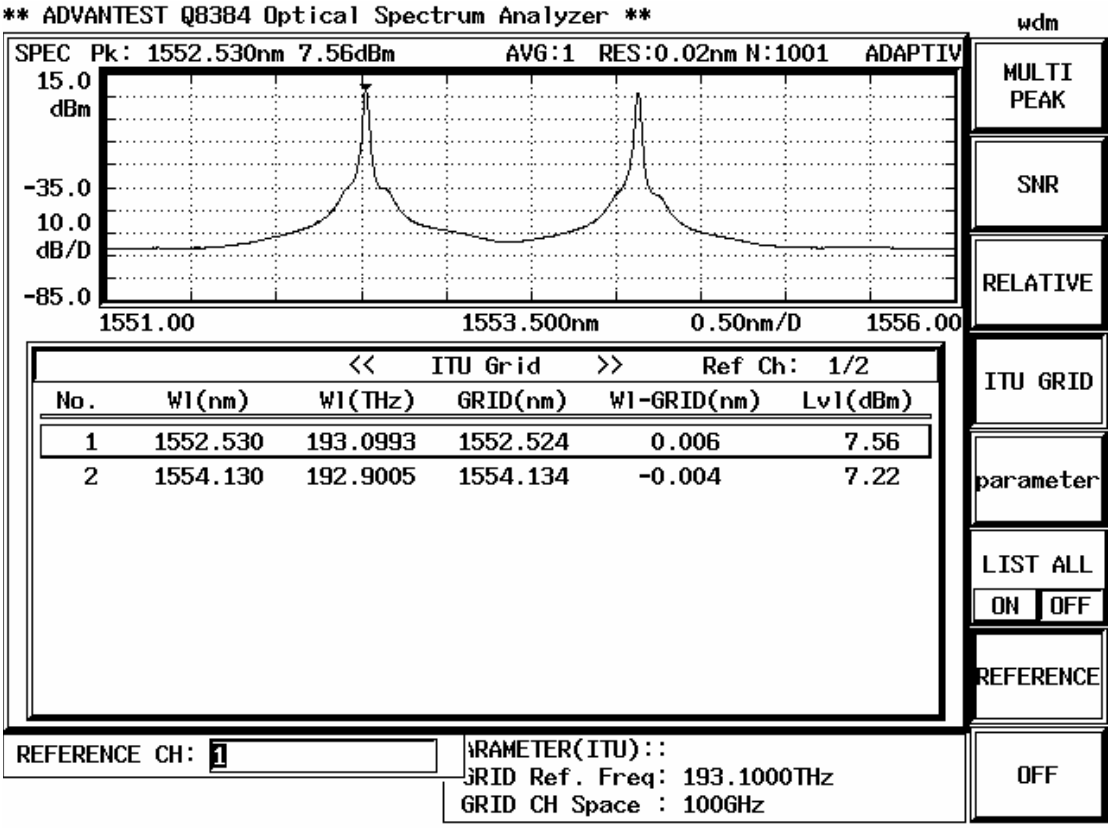

Figure 5.4 A screen capture from the Advantest Q8384 optical spectrum analyzer illustrating the results of peak power and output wavelength measurements at the output of the optical multiplexer.

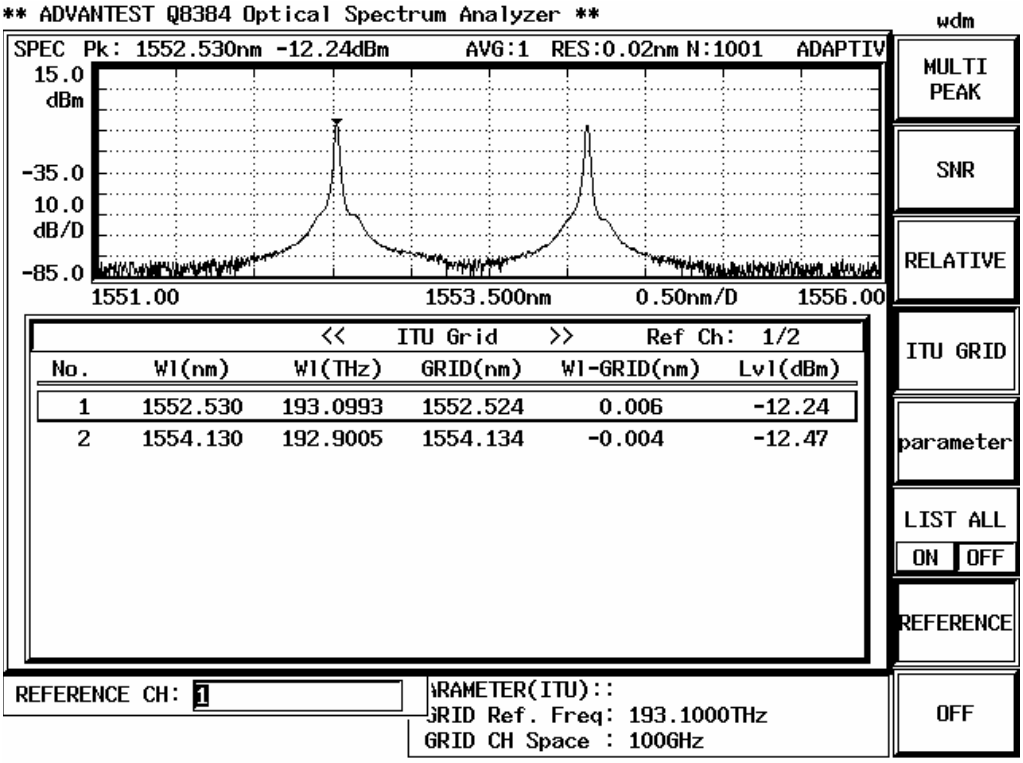

Figure 5.5 A screen from the Advantest Q8384 optical spectrum analyzer illustrating the results of peak power and output wavelength measurements at the input of the optical demultiplexer.

5.3.2 Transmission Response Measurements and Analysis

RF transmission response measurements provide plots of the RF gain, or loss in a communications channel over a specified frequency range. The vector network analyzer plots the output trend over the operating frequency range using

$$Transmission(dB) = 10\log\left(\frac{p_{trans}}{P_{inc}}\right) \quad (5.1)$$

where P_{trans} is the RF power received at the output of the receiver and P_{inc} is the RF power transmitted at the input to the laser transmitter. Major factors that can impact the value of the gain through an analog FSO communications channel are noise, optical attenuation, electrical-optical-electrical conversions, and insertion losses. Sources of noise, as explained in Chapter 2, are relative intensity noise (RIN) generated by the analog laser transmitter, shot noise generated by the photodiode in the analog receiver, and thermal noise generated by resistors in the transceiver circuitry. Optical attenuation due to propagation through the free-space channel increases proportionally with the distance. Electrical-optical-electrical conversions introduce a steady amount of loss that can be added to the gain of the FSO communications channel and is independent of link length. Optical insertion losses for commercial FSO links are added through the coupling mechanism between the FSO transmitting/receiving telescopes and the optical fibers that lead to the transceivers. These coupling losses are responsible for a considerable amount of insertion loss.

To compensate for these losses and extend the FSO link length, optical or RF amplifiers may be inserted. An optical amplifier added after the analog laser modulator can boost the optical power level reaching the detector, while an RF

amplifier connected after the analog receiver can boost the RF power level reaching an RF receiver.

Results of the transmission response measurements for Ch29, with and without the RF amplifier included, are shown in Figure 5.6. Without the RF amplifier, the transmission response (loss) varied from -23.07 dB to -16.05 dB over the operating frequency range 55-870 MHz. With the RF amplifier, the transmission response (gain) varied from 4.27 dB to 8.98 dB over the same frequency range.

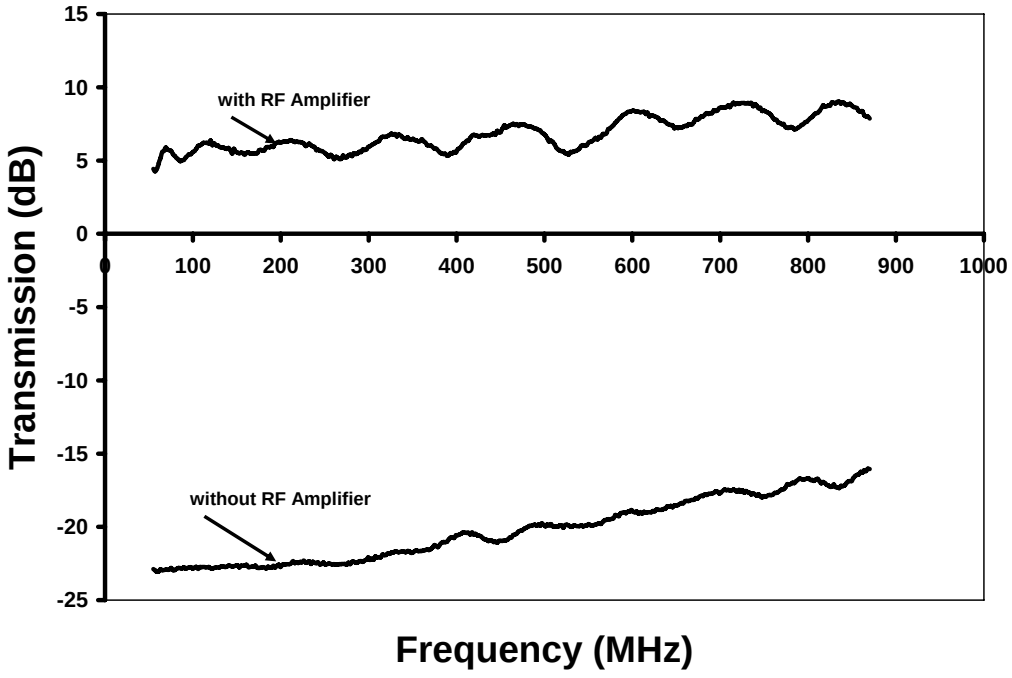

Figure 5.6 Results of transmission response measurements for Ch29, 1554.134 nm.

Figure 5.7 illustrates the results of the transmission response measurements for Ch31. Similarly, without the RF amplifier, the transmission response changed from -23.44 dB to -16.789 dB over the operating frequency range 55-870 MHz. With the RF amplifier, the transmission response changed from 4.23 dB to 8.38 dB over the same frequency range.

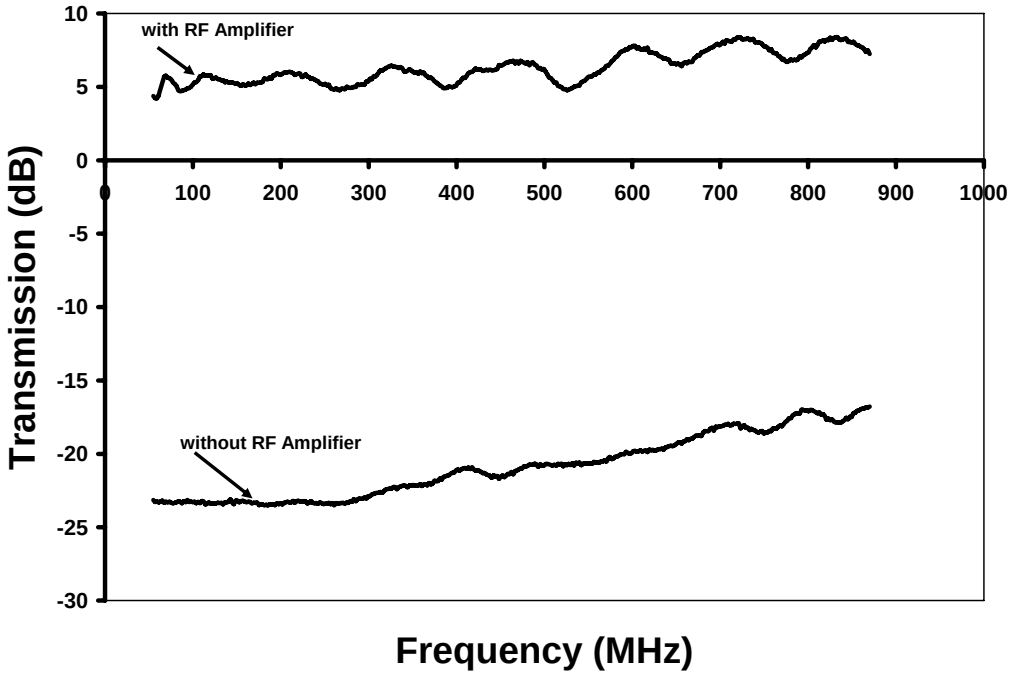

Figure 5.7 Results of transmission response measurements for Ch31, 1552.524nm.

These measurements for both multiplexed channels compare favorably with the -20 to -50 dB losses reported in other measurements for analog fiber optic channels [40]. The RF amplifier provides more power gain allowing the FSO signal to offset the FSO losses, thus allowing increased link lengths.

5.3.3 *Signal-to-Noise Ratio (SNR) Measurements and Analysis*

SNR is an important measure of the performance of communications links with respect to the existing noise. For this examination, SNR measurements were carried out on the FSO link, with and without the RF amplifier, over a frequency range of 55-870 MHz. The RF output power from the signal generator was 0 dBm for all measurements. The results of the SNR measurements for Ch29 are shown in Figure 5.8. Without the RF amplifier, the SNR starts at a lowest value of 14.18 dB at 55 MHz and increases to a highest value of 42.21 dB at 870 MHz. With the RF amplifier, the SNR starts out at a lowest value of 39.99 dB at 55 MHz and increases to a highest value of 65.46 dB at 850 MHz.

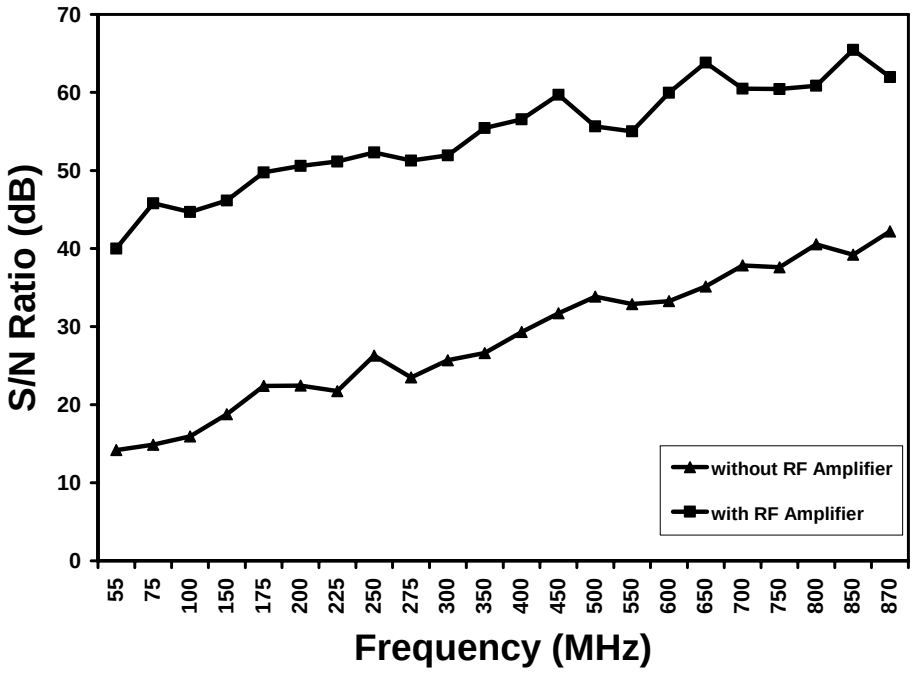

Figure .5.8 Results of SNR measurements for Ch29, 1554.134 nm.

Results of the SNR measurements for Ch31 are shown in Figure 5.9, with and without the RF amplifier included. Without the RF amplifier, the SNR fluctuated from 12.9 dB to 41.23 dB over the operating frequency range of 55-870 MHz. With the RF amplifier, the SNR fluctuated from 39.01 dB to 59.23 dB over the same frequency range. These measurements for both multiplexed channels compare positively with results from SNR measurements on other analog fiber optic links as reported in [40]. Thus, FSO appears a viable alternative for optical fiber in short distance applications.

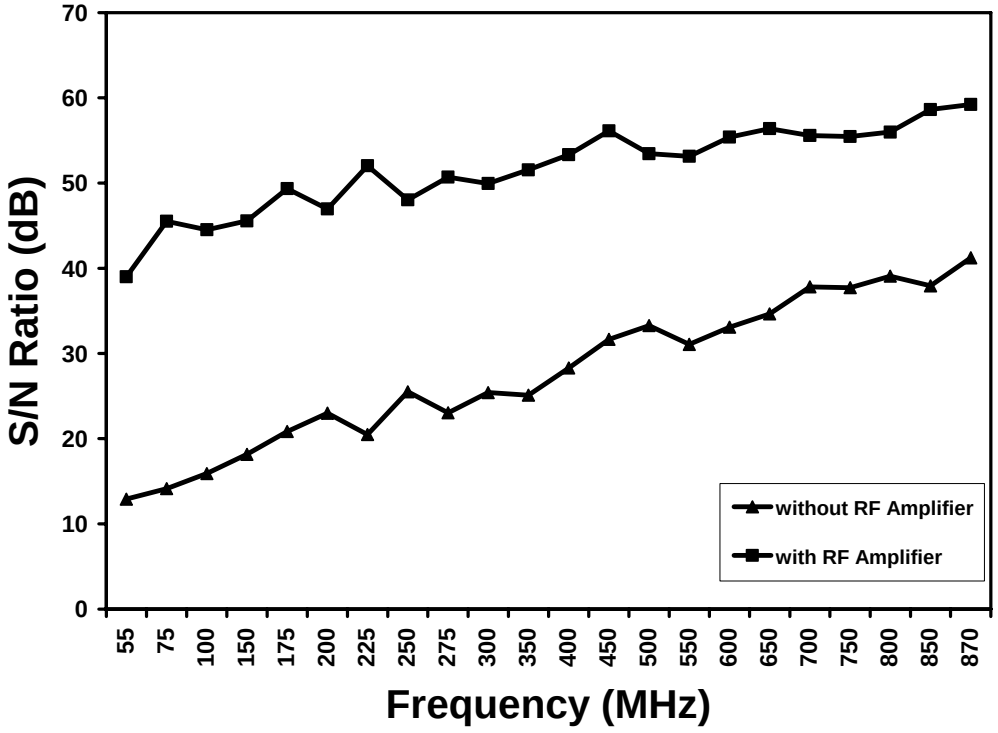

Figure 5.9 Results of SNR measurements for Ch31, 1552.524 nm.

5.3.4 Dynamic Range Measurements

Typical CATV signals are composed of a number of RF carriers over a single communications channel and it is important to predetermine the dynamic range of the channel to insure that harmonic distortion does not arise and lead to undesired frequency overlap. Harmonic distortion is normally not of great concern for single carrier channels.

There are two main methods to measure the dynamic range, as mentioned in Chapter 3. Identically, the second method was used to measure the dynamic range in this study. The third order intermodulation (3IM) power was plotted to provide the third order intermodulation free dynamic range. An RF mixer was used to multiplex two equal power RF signals at closely spaced frequencies of $f_1 = 499\ MHz$, $f_2 = 501\ MHz$. Providing the composite RF signal into the FSO channel, the 3IM signal power was measured at frequencies $2f_1 - f_2 = 497\ MHz$, *and* $2f_2 - f_1 = 503\ MHz$. Repeating the same measurements while increasing the input power for both frequencies allows the 3IM line to be plotted. Measuring the output power of the fundamental frequency $f = 500\ MHz$ over the same range of input power plots the fundamental output line, which intersects the 3IM line. In this study, a directly modulated, distributed feedback (DFB) laser diode was utilized as the transmitter, so RIN is the dominant noise source.

Using the second method, the 3IM free dynamic range for Ch29 was 95 dB.Hz$^{2/3}$, as shown in Figure 5.10.

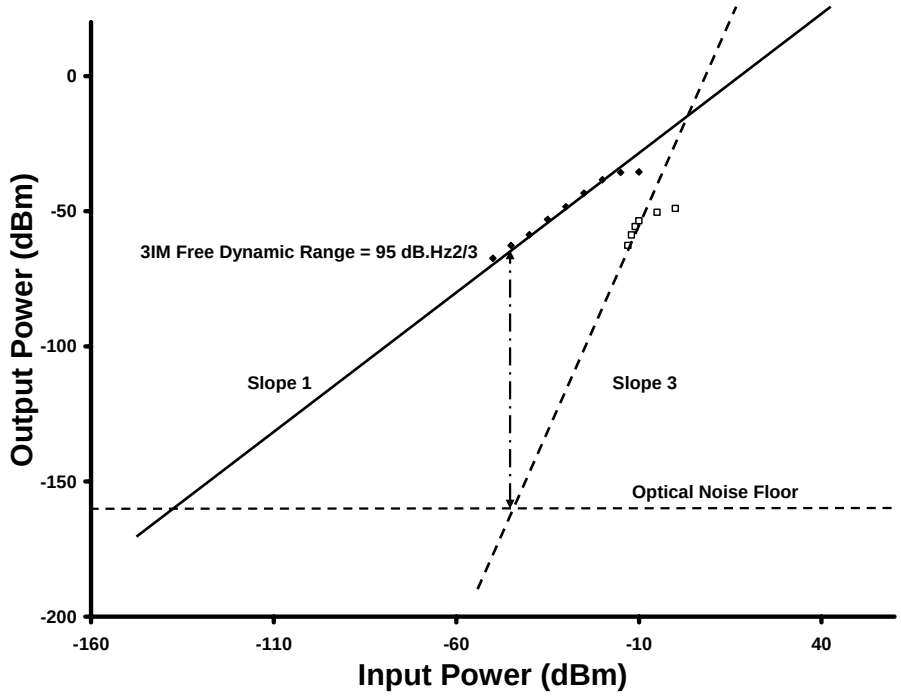

Figure 5.10 Results of 3rd order intermodulation free dynamic range measurements for Ch29.

Also, the 3IM free dynamic range for Ch31 is 92 dB.Hz$^{2/3}$, as shown in Figure 5.11. Compared with previously reported results for optical fiber links, the 3IM free dynamic ranges measured over the FSO link are sufficient to allow a distortion free FSO communications channel for CATV applications.

Linearization of the modulator can enhance the analog channel performance by reducing the signals produced by harmonic distortion. Analog electronic correction of the distorted electro-optic devices, correction by digital signal processing, and optical linearization are three current methods of linearization [10]. The simplest linearization method is to use a narrowband filter at the output of the analog modulator to allow the frequencies $2f_1 - f_2$ *and* $2f_2 - f_1$ to pass and eliminate the rest of the 3rd order distortion signals.

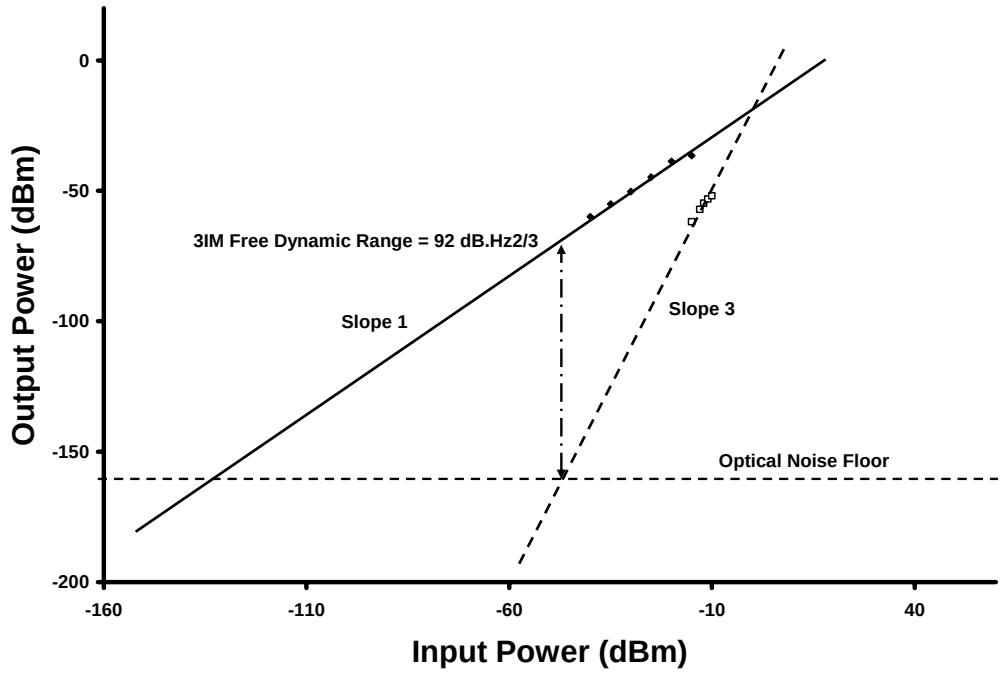

Figure 5.11 Results of 3rd order intermodulation free dynamic range measurements for Ch31.

5.4 Summary

This chapter has reported the results of an investigation into the use of FSO technology for potential CATV application. The results of optical power, transmission response, SNR, and dynamic range measurements indicate the suitability of FSO links. The motivation for this investigation has been to take advantage of the characteristics of FSO technology for the deployment of CATV links in metropolitan areas.

Chapter 6

Conclusions and Future Work

6.1 Conclusions

The major of focus of this dissertation research was the investigation of the effectiveness of FSO to transport analog radio frequency (RF) intensity-modulated signals. The experimental results, supported and verified with theoretical analysis, showed that FSO provides a viable transmission medium in antenna-remoting applications, as well as cellular networks and cable television (CATV) signal distribution networks.

The *advantages* of transmitting modulated radio frequency (RF) signals over FSO links are as follows:

- FSO transmission links can be deployed *faster*, in some instances more *economically*, and provide a faster return on investment than optical fiber links.
- When compared with wireless RF links, FSO requires *no licensing*, provides better link *security* and much higher *immunity* to electromagnetic interference (EMI).
- FSO is highly *invulnerable* to interference from other sources of laser radiation.
- Size and weight saving is an important seek for particular applications of laser communications, such as satellite-to-airplane or airplane-to-airplane laser

communications. Analog FSO can reduce the cost, weight, and size of transmission equipment as compared to a digital implementation by eliminating the needs to analog-digital-analog converters.

The contributions of this work are the experiment results and conclusions that follow, indicating that FSO provides a suitable transmission medium for radar signals, for transporting *IS-95 CDMA* signals to base stations from macro-and microcell sites, and for the deployment of *CATV* links. To the best of the author's knowledge, these are the first reported results of their kind.

First, the study showed comparisons of FSO performance with that of an identical fiber optic link. The motivation for the comparison was the assurance of more accurate comparison, which indicates the potential improvements that can be conducted to develop better FSO link performance. This study provided measurements of optical power, transmission response, reflection response, group delay that defines phase distortion, carrier-to-noise ratio (CNR), and dynamic range that defines nonlinear distortion. These measurements established the characteristics of analog FSO link as follows:

- Optical loss, RF gain, and RF SNR for analog FSO links compare favorably with those of analog fiber-optic links
- Similar to fiber-optic links, analog FSO links do not introduce phase distortion.

- The dynamic range of the analog FSO link was good enough to provide a distortion free communications channel.

From these results, the viability of FSO as an alternative to fiber can be more firmly established.

Second, a new method to setup temporary IS-95 CDMA microcells or permanent IS-95 CDMA macrocells using FSO was proposed. Experimental measurements of user power and SNR indicate that the mobile unit was continuously connected to its respective base station through FSO link connecting the cell. Also, this mobile unit has not shown any intention to hand off to another base station while it is presented within the cell coverage area. Moreover, this study showed the suitability of replacing an expensive directional microwave connection which is usually installed to set up temporary microcell with an economic FSO connection. Further, the viability of the method was demonstrated in the laboratory.

Third, the demonstration of a new transmission technique of multiple radio frequency (RF) signals, e.g., CATV signals, over a single FSO link using wavelength division multiplexing (WDM) technology. The results supported with theoretical analysis, of optical power, transmission response, SNR, and dynamic range measurements indicate the suitability of FSO links for multiple radio frequency applications. Although FSO links contain nonlinear devices which can create distortion signals at

the link output, this investigation showed that the FSO measured dynamic range is sufficient to allow distortion free transmission of multiple carriers.

6.2 Future Work

This investigation has led to ideas for additional, future research. All of the previously described experiments were performed on a FSO link set up indoors in a laboratory environment. From a more practical perspective, it may prove useful to repeat the study on an outdoor installation where the link length is several hundred meters and subject to weather conditions that are difficult to replicate in the lab.

Also, this investigation showed that the optical loss for the simultaneous transmission of multiple RF signals over a single FSO link using wavelength division multiplexing (WDM) technology is larger than that of the transmission of single RF signal over FSO link. The reason for this additional optical loss was not clear and was left as a topic for future investigation.

In addition, this investigation demonstrated the viability of using FSO link to transport IS-95 CDMA signals, but there is still needs to be an investigation into the transport of GSM signals.

BIBLIOGRAPHY

[1] D. Killinger, “Free space optics for laser communication through the air,” *Optics & FPhotonics News*, pp. 36-42, October 2002.

[2] M. Gebhart, E. Leitgeb, U. Birnbacher, and P. Schrotter, “Ethernet accesss network based on free-space optic deployment technology,” Free-Space Laser Communication Technologies XVI, Proc. SPIE Vol. 5338, p. 131-142, 2004.

[3] Y. Hu, R. Cai, and C. Xue, “Broadband wireless optical network technology,” Proc. SPIE Vol 5282, p. 827-834, Network Architectures, Management, and Applications, 2004.

[4] E. Leitgeb, J. Brengenzer, M. Gebhart, P. Fasser, and A. Merdonig, “Free-space optics: broadband wireless supplement to fiber networks,” Proc. SPIE Vol. 4975, p. 57-68, Free- Space Laser Communication technologies XV, 2003.

[5] F. Jiang, M. Gong, H. Zhang, P. Yan, K. Zhang, X. Yang, and W. Jin,”Data transmitting and receiving technologies for free-space optical communications,” Proc. SPIE Vol. 4908, Metro and Access Networks II, 2002.

[6] J. Pan, M. evans, T. Euler, H. Johnson, and F. DeNap, ”Free-Space optical communications: opportunities and challenges from carrier’s perspective,” Proc. SPIE Vol. 4911, p. 58-72, Wireless and Mobile Communications II, 2002.

[7] S. Bloom, W. Hartley, “Hyprid FSO Radio (HFR): some preliminary results,” Proc. SPIE Vol 4873, p. 143-154, Optical Wireless Communications V, 2002.

[8] V. Sidorovich,“ Solar background effects in wireless optical communications,” Proc. SPIE Vo. 4873, p. 133-142, Optical Wireless Communications V, 2002.

[9] K. Williams, L. Nichols, and R. Esman, “Photodetector nonlinearity limitations on a high-dynamic range 3 GHz fiber optic link,” *J. Lightwave Technol.*, 16, 192-9, 1998.

[10] C. H. Cox, III, *Analog Optical Links Theory Practice*, Cambridge, Cambridge University Press, New York, 2004.

[11] Hakki. H. Refai, James J. Sluss, Jr., Mohammed Atiquzzaman, Hung Nguyen and Duc Ngo, “The application of fiber optic wavelength division multiplexing in RF avionics,” Proceedings of the 23rd Digital Avionics Systems Conference (DASC), Salt Lake City, UT, October 24-28, 2004, pp. 8.D.1-1 to 8.D.1-8.

[12] E.Ackerman, D. Kasemset, S. Wanuga, D. Hogue, and J. Komiak, “A high-gain directly modulated L-band microwave optical link,” *IEEE MTT-S Int. Microwave Symp.* Dig., Dallas, Texas, pp. 153-5, 1990.

[13] C. Cox, H. Roussell, R. Ram, and R. Helkey, “Broadband, directly modulated analog fiber optic link with positive intrinsic gain and reduced noise figure,”

Proc. IEEE International Tropical Meeting on Microwave Photonics, Princeton, New Jersey, 1998.

[14] C. Cox, E. Ackerman, and G. Betts, "Relationship between gain and noise figure of an optical analog link," *IEEE MTT-S Int. Microwave Symp*. Dig., San Francisco, California, pp. 1551-4, 1996.

[15] E. Ackerman, C. Cox, G. Betts, H. Roussell, K. Ray, and F. O.'Donnell," Input impedance conditions for minimizing the noise figure of an analog link," *IEEE Trans. Microwave Theory Tech*., 46, 2025-31, 1998.

[16] W. Bridges and J.Schaffner, " Distortion in linearized electro-optic modulators," *IEEE Trans. Microwave Theory Tech.*, 43, 2184-97, 1995.

[17] G. Betts, "Linearized modulator for suboctave-bandpass optical analog links," *IEEE Trans. Microwave Theory Tech.*, 42, 2642-9, 1994.

[18] Hakki H. Refai, James. J. Sluss, Jr., and Hazem H. Refai, "Optical interference on free- space optical transceivers," *Frontiers in Optics – 87th Optical Society of America Annual Meeting*, Tucson, AZ, October 5-9, 2003- pp. WJJ6.

[19] Hakki H. Refai, James J. Sluss, Jr., and Hazem H. Refai, "Free-space optical communication performance in the presence of interfering laser signals," Proceedings of the SPIE Defense and Security Symposium 2005,Vol. 5793, Orlando, FL, March 18–April 1, 2005.

[20] J. Wu, J. Wu, and H. Tsao, “A radio-over-fiber network for microcellular system application,” IEEE Trans. Vehicular Technology, 47, 84-94, 1998.

[21] S. Ozer, and S. Papavassiliou, ”Performance analysis of CDMA systems with integrated services,” IEEE Trans. Vehicular Technology, 52, pp. 823-836, 2003.

[22] J. Fan, C. Lu, and L. Kazovsky, ”Dynamic range requirements for microcellular personal communication systems using analog fiber-optic links,” IEEE Trans. Microwave Theory Tech., 45, pp. 1390-1397, 1997.

[23] T. Darcie and G. Bodeep, “ Lightwave subcarrier CATV transmission systems,” *IEEE Trans. Microwave Theory Tech*., 38, 524-33, 1990.

[24] G. Wilson, T. Wood, M. Gans, J. Sulhoff, J. Johnson, T. Tanbun-Ek, and P. Morton, “Predistortion of Electroabsobtion modulators for analog CATV systems at 1.55 Mm,” IEEE J. Lightwave Technology, 15, 1654-1662, 1997.

[25] Hakki H. Refai, James J. Sluss, Jr., Hazem H. Refai, and Mohammed Atiquzzaman, “Transporting RF signals over free-space optical links,” Proceedings of the SPIE Photonics West 2005, San Jose, CA, January 22- 27, 2005.

[26] Hakki H. Refai, James J. Sluss, Jr., Hazem H. Refai, and Mohammed Atiquzzaman, “A comparative study of performance of analog fiber-optic links versus free-space optical links,” Accepted to SPIE Optical Engineering.

[27] Hakki H. Refai, James J. Sluss, Jr., and Hazem H. Refai, "The use of free-space optical links for CATV applications," Proceedings of the SPIE Opto Ireland, Dublin, Ireland, April 4-5, 2005.

[28] Hakki H. Refai, James J. Sluss, Jr., and Hazem H. Refai," The transmission of multiple RF signals in free-space optics using wavelength division multiplexing," Proceedings of the SPIE Defense and Security Symposium 2005, Orlando, FL, March 18–April 1, 2005.

[29] Hakki H. Refai, James. J. Sluss, Jr., Hazem H. Refai, "Interconnection of IS-95 CDMA microcells using free-space optical links," Proceedings of the 1st IEEE and IFIP International Conference on Wireless and Optical Communications Networks (WOCN 2004), Muscat, Oman, June 7-10, 2004, pp. 78-81.

[30] Gerd Keiser, *Optical fiber communications*, third edition, McGRAW-HILL, 2000.

[31] H. Willebraund and B. S. Ghuman, *Free-space optics: enabling optical connectivity in today's networks,* SAMS, 2002.

[32] S.O. Kasap, *Optoelectronics and photonics; principle and practices,* Prentice Hall, 2001.

[33] Y. Yamamoto, "AM and FM quantum noise in semiconductor lasers- Part I: Theoretical analysis," IEEE J. Quantum Electron, 19, 34-46, 1983.

[34] Y. Yamamoto, S. Saito, and T. Mukai, ”AM and FM quantum noise in semiconductor lasers- Part II: Comparision of theoretical and experimental results for AlGaAs lasers,” IEEE J. Quantum Electron, 19, 47-58, 1983.

[35] H. A. Willebrand and B. S. Ghuman, “Fiber optics without fiber,” IEEE Spectrum, Volume: 38, No: 8, Aug. 2001, pp. 43.

[36] W. E. Stephens and T. R. Joseph, “System characteristics of direct modulated and externally modulated RF fiber-optic link,” *IEEE Journal of Lightwave Technology*, Vol. LT-5, No. 3, pp. 380-387, March, 1987.

[37] C. H. Cox, E. Ackerman, R. Helkey, and G. E. Betss, “Direct-detection analog optical links,” *IEEE Transactions on Microwave Theory and Techniques*, Vol. 45, No. 8, August 1997.

[38] S. L. Woodward, and Sirikat Ariyavisitakul, Transporting CDMA signals over an analog optical link, *IEEE Transactions on Vehicular Technology*, Vol. 48, No. 4, July 1999.

[39] Vijay K. Garg, *Wireless Network Evolution 2G to 3G*, Prentice Hall PTR 2002.page 230, 279, 281

[40] C. H. Cox III, G. E. Betts, and L. M. Johnson, “An analytic and experimental comparison of direct and external modulation in analog fiber-optic links,” *IEEE Transactions on Microwave Theory and Techniques*, Vol. 38, No. 5, pp.501-509, May 1990.

Appendix

Data of measurements for the figures

Please check the contents of the included CD.